Copyright

by

Lucas Melo Monteiro

2019

The Thesis Committee for Lucas Melo Monteiro
Certifies that this is the approved version of the following Thesis:

Characterization of Gulf of Mexico Clay at Low Effective Normal Stresses for Offshore Pipeline Applications

APPROVED BY
SUPERVISING COMMITTEE:

Robert B. Gilbert, Supervisor

Jorge G. Zornberg

Characterization of Gulf of Mexico Clay at Low Effective Normal Stresses for Offshore Pipeline Applications

by

Lucas Melo Monteiro

Thesis

Presented to the Faculty of the Graduate School of

The University of Texas at Austin

in Partial Fulfillment

of the Requirements

for the Degree of

Master of Science in Engineering

The University of Texas at Austin

May 2019

Dedication

To my parents, Luis Carlos de Sousa Monteiro and Adriana Melo Monteiro, my brothers, Tiago Melo Monteiro and Matheus Melo Monteiro, and my daughter, Maria Clara Pinheiro Melo.

Acknowledgements

I would like to express my appreciation and gratitude to my supervisor, Dr. Robert B. Gilbert, for his valuable guidance and support during this research. I would also like to thank Dr. Jorge Zornberg for advising and reviewing this thesis. Additionally, I would like to extend my thanks to Dr. Jinbo Chen for his valuable technical advising throughout every step of this research.

I would also like to express my thanks to others geotechnical engineering faculty members, Dr. Cox, Dr. El Mohtar, and Dr. Kumar for their technical contribution in the courses taken throughout the completion of this degree.

I could not be grateful enough to have had the opportunity to work with such brilliant classmates during this research, so my sincere thanks to Chihun Sung, Dr. Yunhan Huang, Ahmed Hussien, Jonas Bauer and James Munson.

Additionally, I would like to thank all the amazing friends I had the opportunity to meet in Austin, in special to my dear classmates Antonios Alvertos, Ashim Gajurel, Hratch Agopian and my roommate Konstantinos Sitaropoulos. My staying in Austin would not have been as amazing as it was without your friendship.

Lastly, I would like to express my deepest gratitude to my parents, my brothers, and my daughter, who have been and will always be with me in every step of my life.

Abstract

Characterization of Gulf of Mexico Clay at Low Effective Normal Stresses for Offshore Pipeline Applications

Lucas Melo Monteiro, M.S.E.

The University of Texas at Austin, 2019

Supervisor: Robert B. Gilbert

Pipelines and flowlines represent a major cost in offshore oil and gas operations. The initial embedment of the pipeline during laying influences the pipeline service resistance to axial and lateral motion and is dependent on the strength of the supporting soil at low effective normal stresses. This study aims to characterize Gulf of Mexico clay at low effective normal stresses in different scenarios. T-bar tests are performed to estimate the undrained shear strength of the clay. Embedment tests are conducted to estimate the initial penetration of pipes and consolidation after laying. Tilt-table tests are carried out to measure the drained residual interface strength between pipeline coating and Gulf of Mexico clay from three different offshore sites. T-bar results indicate that thixotropy of the clay has an impact on the undrained shear strength shortly after the clay is remolded and, after approximately 72 hours, a large portion of the increase in the undrained shear strength of the clay due to thixotropy occurs, with the sensitivity of the clay being about 2. For values greater than 1.5, the sensitivity seems to slightly decrease with depth. Embedment test results indicate that methods commonly used in practice to predict the initial

penetration of pipelines agree well with model tests performed with a 3-ft long pipe section and provide a reasonable starting point for larger sections (i.e. 10-ft long). Additionally, consolidation following installation plays an important role in the final embedment of pipes. The c_v and C_c of the clay are estimated to be approximately 0.009 ft^2/day (0.3 m^2/year) and 0.71 to 1.26 (average value of 0.78), respectively. Results from tilt-table tests using stresses lower than 150 psf (7.2 kPa) indicate that 1) the interface residual strength is mobilized at about 1 to 2 in (25 to 50 mm) of shear displacement; 2) the Mohr-Coulomb failure envelope is non-linear for very low effective normal stresses and the curvature becomes flatter as the stress increases; 3) the drained residual strength at the interface depends on the composition of the clay and; 4) similar coatings obtained from different manufacturers may present minor differences in performance under similar stress conditions.

Table of Contents

List of Tables

List of Figures

Chapter 1: Introduction

1.1 MOTIVATION

The development in offshore facilities have increased substantially over the last decades in face of the escalating demand of energy around the world. Offshore structures encountered in oil and gas facilities and in renewable energy systems have been constantly improved in respect to design and installation.

The developments in the oil and gas industry are usually associated with moored floating facilities, which are chained to the seabed via an anchoring system (Randolph et al. 2011). During operation of an offshore platform, the hydrocarbons are transported from the wells to in-field processing facilities and to shore by flowlines (usually the flowlines that transport the processed product from the processing facility to the shore are known as pipelines). As offshore developments extend far from the shore, pipelines and risers (usually vertical pipes that transport hydrocarbons from the seabed to a fixed or floating facility above the sea surface) represent an important part of the project, with costs being significant in the overall field development, typically exceeding US $4 million per km on the North-West Shelf of Australia, for example. (Randolph and Gourvenec, 2011).

Pipelines are designed to achieve stability under hydrodynamic loading from waves and currents, possible external loading interaction with anchor lines, iceberg movements and mass transport (i.e. submarine slides and debris flows), and due to expansion and contraction caused by successive cycles of startup (hydrocarbon is transported) and shutdown (no transport of hydrocarbon), which cause a phenomenon known as pipeline walking (Randolph and Gourvenec, 2011). A few of the parameters that go into a pipeline design are an adequate characterization of the seabed soil, the initial pipeline embedment

(also known as as-laid embedment) and the interface strength between the pipeline and the seabed soil during axial movement (pipeline walking).

Pipelines are usually laid on the seabed, and its embedment is a combination of its self-weight and contact stresses acting in the touchdown zone during layering operation, which is heavily influenced by the dynamic motion of the pipe generated as it encounters with the seabed soil. The amount of embedment is of great importance since it influences the pipeline service resistance to axial and lateral motion. Since the amount of embedment depends on the strength of the seabed soil, accurate characterization of the seabed at shallow depths is of great importance and challenging due to the very low effective stresses, causing the soil to behave outside the common experience of geotechnical design (White and Randolph, 2007).

The axial resistance provided by the supporting soil during axial movement of the pipelines is a key component to adequate design of the pipeline against lateral buckling and pipeline walking. The magnitude of the axial resistance depends on the rate and duration of the loading and the magnitude of the axial movements. After successive cycles of startup and shutdown, since the shear displacements along the surface can assume large values, it is assumed that the strength of the interface between the pipeline and the supporting soil reach drained conditions and assumes its residual value. The axial soil resistance can be estimated by an interface friction which represented the friction developed between the pipeline coating and the supporting soil (Najjar et al. 2007).

Two challenges are identified in measuring the drained interface strength in a laboratory test. First, the effective normal stresses acting on the interface are typically less than 100 psf (5 kPa), which is very low if compared to the conventional laboratory test methods used to measure shear strength, such as direct shear tests and triaxial tests. Second, the soil (marine clays) usually have a small coefficient of consolidation, which means that

small shear rates must be used in order to drained conditions be achieved at the interface (Najjar et al. 2003).

This study focuses on characterizing the behavior of marine clays under low effective normal stresses, by means of adequately characterizing its intact and remolded undrained shear strength, which is used to estimate the amount of embedment of a pipe when laid on the clay. Additionally, a tilt table method is presented to estimate the friction developed at the interface between a pipeline coating surface and marine clay when subjected to low effective normal stresses.

1.2 OBJECTIVES

The main objectives of this research are:

1. Characterize the undrained shear strength of Gulf of Mexico clay by performing T-bar tests. Based on the undrained shear strength measurements, estimate the clay set-up time for laboratory applications (short periods of time). Additionally, investigate how the remolded undrained strength shortly after the clay is remolded relates to the water content.
2. Estimate the initial embedment of pipes when laid on Gulf of Mexico clay by performing embedment tests and compare the results with the predicted values obtained using equations commonly used in practice. Additionally, estimate the coefficient of consolidation and the coefficient of compression of the clay based on consolidation following pipe laying.
3. Measure the drained residual interface strength between a pipeline coating and Gulf of Mexico clay from three different offshore sites by performing tilt-table tests using different effective normal stresses. The results can be used to estimate the soil-pipe

axial resistance, which is an important parameter to access the overall stability of pipelines.

1.3 STRUCTURE OF THESIS

The introduction is presented in Chapter 1, which includes the motivation, and the objectives of this study. Chapter 2 includes the background information about the topics covered in this research as well as previously published work on T-bar tests, prediction of initial embedment of pipelines and measurement of drained residual interface strength of soils and solid interfaces. Test materials, test program, procedures, discussion of the results and conclusions relative to the T-bar tests, embedment tests and tilt-table tests are presented in Chapter 3, 4 and 5, respectively. A summary of the major conclusions obtained from this study is presented in Chapter 6. The plots of the T-bar tests are presented in the Appendix A. Additional information about the tilt-table tests results are presented in Appendix B.

Chapter 2: Literature Review

2.1 Introduction and Objectives

This chapters presents background information about characterization of marine clays response under different scenarios. The goal is to provide information about how the undrained shear strength of marine clays can be measured, focusing on T-bar tests. Additionally, information about the laying process of offshore pipelines and methods of estimating the initial pipe embedment on marine clays is described. Moreover, a summary of published work on available tests that can be used to measure the drained residual interface strength between marine clays and solid interfaces is presented.

2.2 Overview about Offshore Geotechnical Engineering

Design practice in offshore geotechnical engineering was born out of the classic onshore geotechnical engineering practice, but the two areas have tended to diverge over the last 30 years, mostly due to the scale of foundations and anchoring elements used offshore, and partly by fundamental differences in construction and installation techniques. Consequently, offshore geotechnical engineering has grown as a specialty and has become an important field of study for professionals and researchers that deal with problems associated with oil and gas development. As example of some of the unique features of this specialty, site investigations in offshore environments are extremely expensive, typically involving several million dollars (Randolph and Gourvenec, 2011). Additionally, soil conditions are often unusual and challenging due to the presence of carbonate soils and corals and, since mobility of infrastructure during installation or operation may cause disturbance followed by "healing" (consolidation in case of clays) of the seabed soil, leading to change in topography and strength (Randolph et al. 2011).

The design of offshore structures is usually very costly mostly due to the combination of environmental loads to be withstood by the structures. Different types of offshore structures are used for oil and gas production and their selection depends on economic and operation considerations, location where the structure will be installed and the operator's interests. The operation of an offshore platform requires the construction and installation structures such as shallow and deep foundations, anchors and pipelines (also known as flowlines) (Richardson et al. 2008).

For the case of pipelines, geotechnical analysis play an important role in assessing the initial embedment of the pipeline after laying, the possible changes in embedment that may occur during the operational lifetime of the pipeline, and the resisting forces that are mobilized between the pipeline and the supporting soil during axial and lateral movements. The geotechnical analysis will directly influence in the chosen route for the pipeline (Randolph and Gourvenec, 2011). A schematic illustration of a typical Deepwater field architecture and flowline network is shown in Figure 2.1.

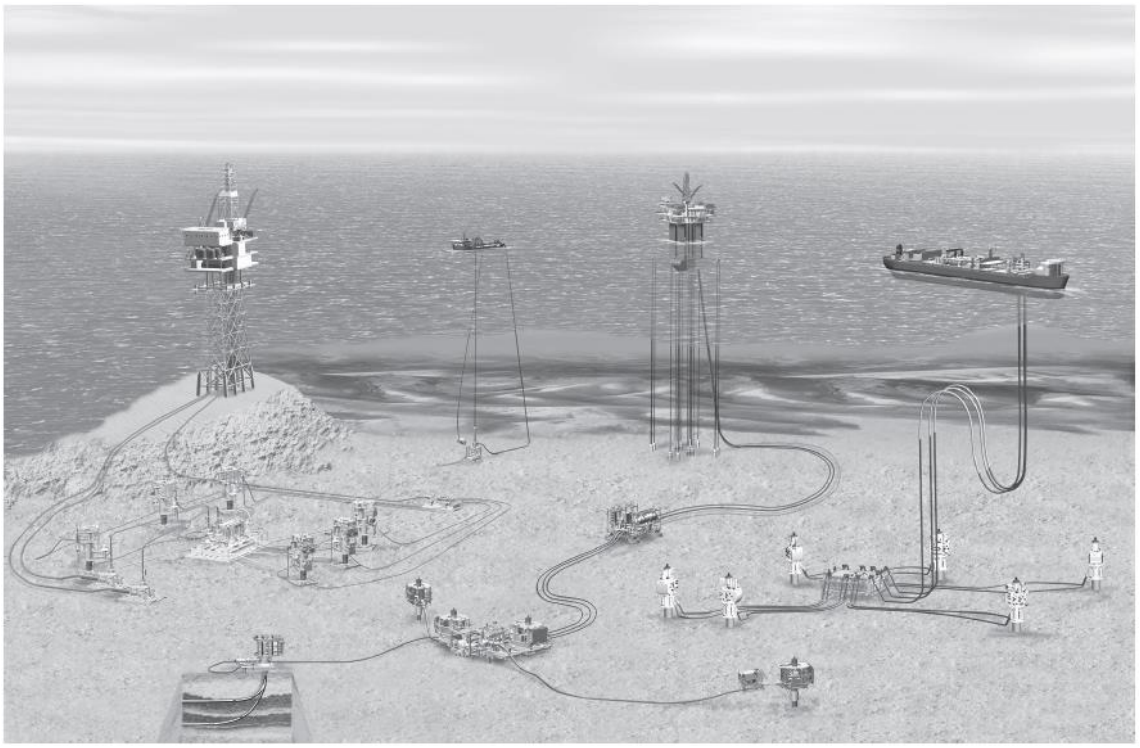

Figure 2.1 Deepwater field architecture (McCarron et al. 2011)

2.3 Available Tests to Measure the Undrained Shear Strength of Marine Clays

In offshore projects, characterizing the soil in order to obtain parameters to be used in design is one of the most important parts of the project. Over the last decade, the geotechnical input parameters used in pipeline design has become more sophisticated, driven by the increased lengths of pipeline needed for remote deep-water developments (Randolph and Gourvenec, 2011). The difficulty associated with obtaining high quality soil samples from deep water locations to be tested in the laboratory increased the necessity to rely on in-situ tests. For shallow depths of soft sediments (usually upper 3-7 ft) there are major challenges associated with measuring the undrained shear strength of the soil, which

are too soft to allow the use of conventional methods to extract “undisturbed” samples, thus, alternative methods must be used in those cases. The most common in-situ tests used to measure the undrained shear strength of clays are: Piezometer Cone Penetrometer Test (CPTU), Vane Shear Test, and full-flow penetrometers tests (T-bar or ball), however, the latter have become accepted as the main test to assess strength of soft sediments at shallow depths for pipeline design (White and Randolph, 2007). An illustration of the T-bar, T-ball and cone penetrometer is shown in Figure 2.2

.

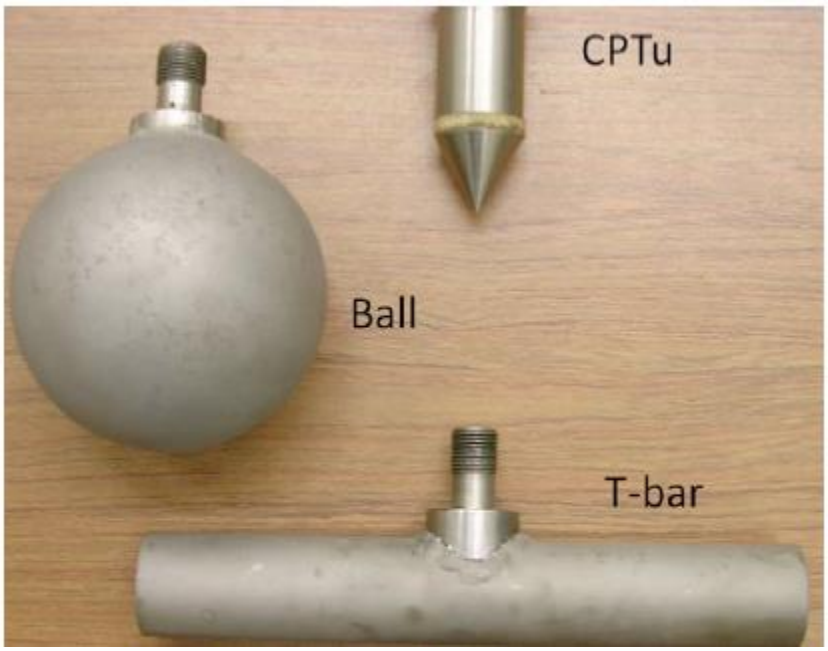

Figure 2.2. T-bar, ball and cone penetrometer (Yafrate et al. 2009)

According to Low et al. (2010), penetration tests such as T-bar and CPTU have a significant advantage over vane shear tests as they provide continuous strength profiles. Additionally, if compared to CPTU, full-flow penetrometer tests provide more accurate

determination of soil resistance due to their projected area, which is normally ten times of the shaft, thus giving ratios of soil resistance to the load from ambient water pressure that are an order of magnitude higher than for any size of cones used in practice. Randolph (2004) cites some advantages of T-bar tests over CPTU: available theoretical solutions for deducing the shear strength from the penetration resistance; the remolded shear strength can be assessed by performing cyclic penetration and extraction of the T-bar.

2.4 T-BAR TESTS

The T-bar consists of a cylindrical bar attached at right angles to a penetrometer rod. A loadcell located at the top of the rod records the differential force on the bar as the rod is inserted into the soil. The recorded undrained penetration resistance (undrained conditions are obtained only if an adequate penetration rate is used), q, is related to the undrained shear strength of the soil by a bearing capacity factor, N_{Tbar} (Stewart and Randolph, 1991).

The original value for N_{Tbar} of 10.5 was proposed by Stewart and Randolph (1994), which was obtained from a plasticity solution for cylinder moving laterally through the soil. Studies performed by several researchers, including Zhou and Randolph (2009), Chung and Randolph (2004), Yafrate et al. (2009) and Low et al. (2010), suggest that a value closer to 11 may be representative for deep penetration. Since the zone of most interest in pipeline design is the upper 1 m, discrepancies in depth datum and load cell zero value should be accounted. Additionally, the bearing capacity factor should be reduced for shallow depths to represented shallow penetration mechanism. According to White and Randolph (2010), N_{Tbar} may be expressed as:

$$N_{Tbar} = N_{Tbar,0} + \frac{\gamma' z}{s_u} \leq N_{Tbar,deep} \qquad \text{(Eq. 2.1)}$$

Where $N_{Tbar,deep}$ is about 11, $N_{Tbar,0}$ is associated with weightless soil at shallow depths and $\gamma' z/S_u$ is the ratio of effective overburden stress to the undrained shear strength of the soil. Values for $N_{Tbar,0}$ lie between 4 and 5 at a penetration of half diameter, and between 6 and 8 at a penetration of 4 diameters (the upper limit corresponds to a fully rough surface of the T-bar while the lower limit corresponds to a smooth surface). For normally consolidated soils, the T-bar factors will reach its deep value ($N_{Tbar,deep}$) within 3 or 4 diameters (depth of approximately 0.5 ft). For cases where a surface crust exists, this depth can double.

For laboratory applications, N_{Tbar} should be adjusted to depths up to 7.5 to 15 diameters (White et al., 2010). According to Eq 2.1, if the undrained shear strength varies linearly with depth (common for normally consolidated clays), the initial bearing capacity factor ($N_{Tbar,0}$) varies linearly until it assumes a value equal to $N_{Tbar,deep}$.

Another parameter that may affect the results obtained from T-bar tests is the rate at which the penetration rod is lowered. Since the undrained shear strength of the soil is of interest, an adequate rate must be used so undrained conditions can be achieved. House et al. (2001) suggests a penetration rate ranging from 0.2 to 0.5 diameters per second, although different rates may be used to account for strain-rate dependency of the penetration resistance, or the onset of consolidation. Dejong et al. (2010) and Norsok (2004) suggest a displacement rate of approximately 0.8 in/s to yield meaningful shear strength values. The penetration velocity can be calculated as a normalized velocity given by the following equation (Finne and Randolph, 1994):

$$V = \frac{vD}{c_v} \qquad \text{(Eq. 2.2)}$$

Where V is the normalized penetration rate, v is the penetration rate and c_v is the coefficient of consolidation of the soil. Studies performed by House et al. (2001), Randolph and Hope (2004) and Norena (2015) indicate that undrained conditions are reached for values of V greater than 10.

T-bar penetrometer tests can also be used to measure the remolded undrained shear strength of soft soils. This is done by performing successive penetration cycles (penetration + extraction) over a short depth interval. Randolph and Gourvenec (2011) suggests that a minimum of 10 cycles should be performed in order to achieve close to fully remolded conditions. Norena (2015) conducted cyclic T-bar tests on soft soil in a centrifuge up until a depth of 5.25 ft (1.6 m) and reached the remolded state after 10 cycles. Lee (2008) performed several cyclic T-bar tests on kaolinite test beds and reported values close to the remolded shear strength after 5 cycles; the values obtained from the 5^{th} cycle were greater than the reconstituted strength, which was attributed to the fact that the T-bar tests in normally consolidated test beds could not fully capture the remolded shear strength because of problems with soil adhering to the T-bar in repeated penetrations. Gerkus (2016) performed cyclic T-bar tests on marine clays test beds and reported that the remolded undrained shear strength was achieved after 4-6 cycles.

Lai (2017) studied the strain effect during penetration by performing T-bar tests with different penetration rates. For a baseline loading rate of 0.8 in/s (for a T-bar with diameter of 1 in), penetration rates higher than 3.2 in/s were found to overestimate the values of undrained shear strength. Figure 2.3 shows the results for all penetration rates.

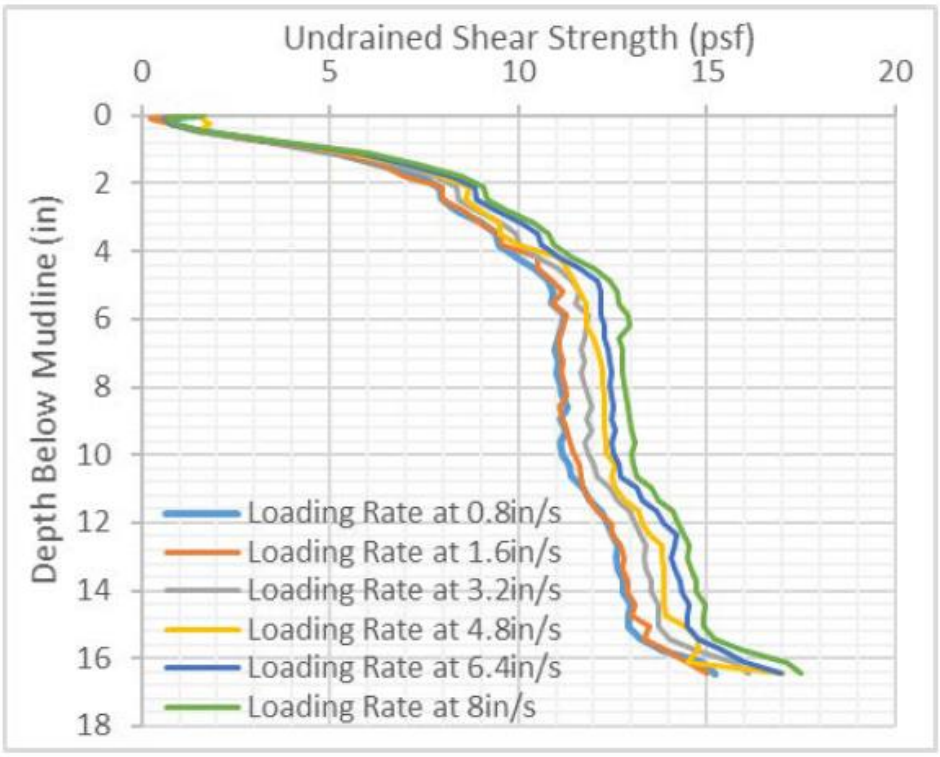

Figure 2.3. Example of S_u profile using different penetration rates (Lai, 2017)

The sensitivity of a soil (S_T) can be estimated by the following equation:

$$S_T = \frac{S_u}{S_{u,rem}} \quad \text{(Eq. 2.3)}$$

Where S_u and $S_{u,rem}$ are the undrained shear strength and the remolded undrained shear strength, respectively. S_T can be obtained by performing cyclic T-bar tests. An example of a soil profile with sensitivity greater than one obtained using cyclic T-bar tests is shown in Figure 2.4.

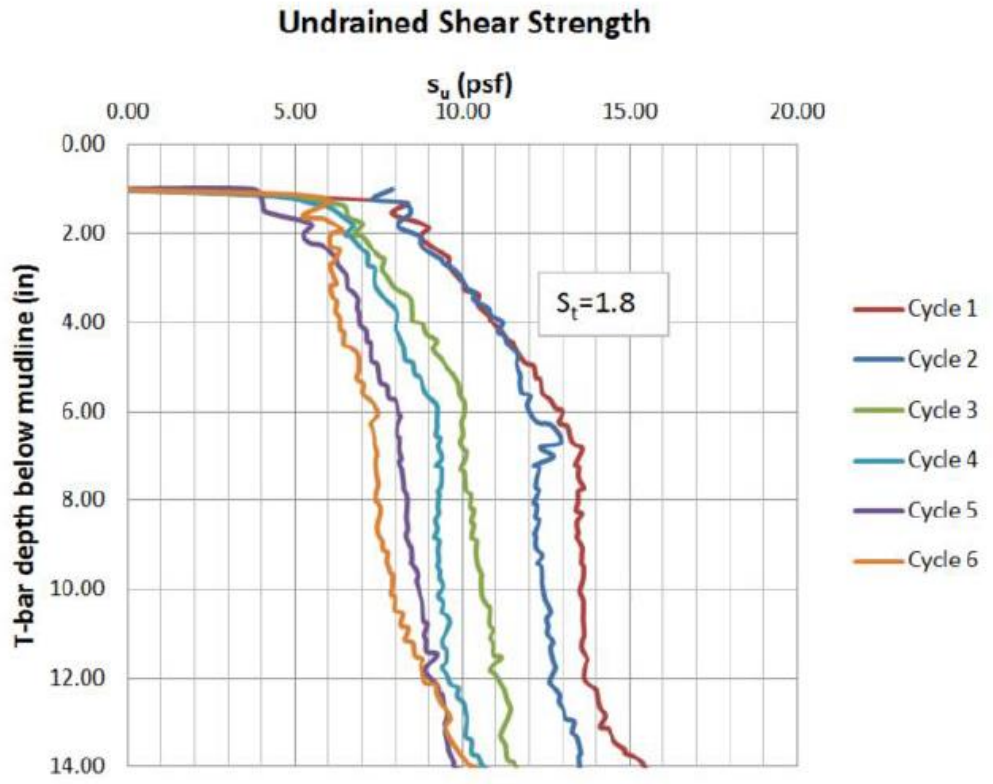

Figure 2.4. Example of soil profile with sensitivity greater than one measured with cyclic T-bar (Gerkus, 2016).

2.5 PIPELINE INITIAL PENETRATION

The initial penetration of pipelines on the seabed strongly influences the overall stability of the pipelines when subjected to axial and lateral movements. Consequently, it should be estimated as accurately as possible. Observations indicate the initial pipeline penetration is greater than the predicted values considering the vertical weight of the pipeline and the bearing capacity of the seabed soil. This additional embedment is due to the stress concentration at the touchdown point and the remolding of the seabed soil due to cyclic movements of the pipeline during the laying process. Those cyclic movements are

caused by movement of the vessel used to lay the pipeline and the hydrodynamic action of the hanging span (Westgate, 2009).

During the laying process, the surrounding soil heaves, which increases the "local" embedment of the pipe. This heave causes an elevation of the soil surface at the shoulders of the pipeline, but it can reduce with time and its contribution to axial and lateral resistance may not be reliable. The nominal embedment of a pipeline is illustrated in Figure 2.5 and it is defined as the pipe-soil contact arc length, p (Simpson et al. 2015).

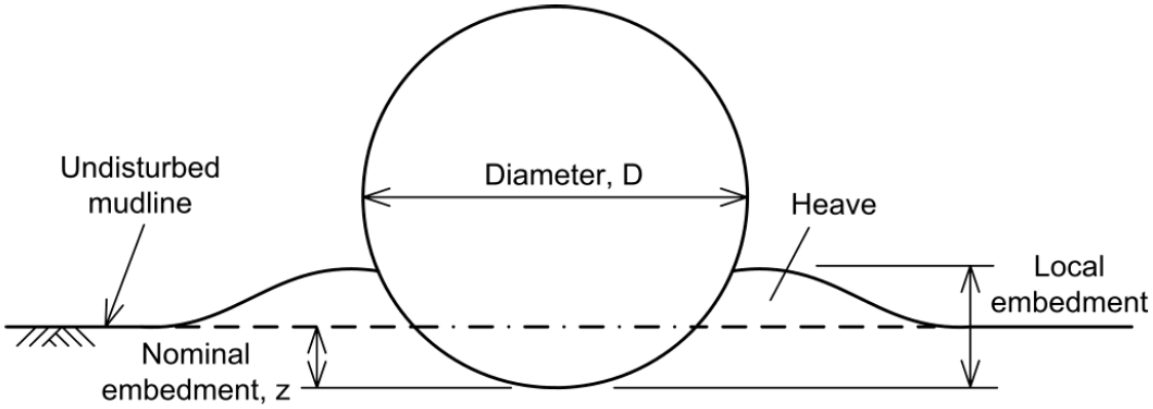

Figure 2.5 Terminology for pipeline embedment (Simpson et al. 2015).

For cases where the seabed soil has low permeability, the laying process can be assessed assuming undrained conditions. A simplified version of a plasticity solution can be used to estimate the initial penetration of a pipeline:

$$\frac{z}{D} = a\left(\frac{V}{DS_u}\right)^b \qquad \text{(Eq. 2.4)}$$

Where z is the initial pipeline embedment, D is the pipeline diameter, V is the weight per unit length, S_u is the undrained shear strength at the pipeline invert (bottom), and a and b are fitting parameters. For shallow depths and smooth pipes, a = 0.007 and b =

2.75 (White and Randolph, 2010). Aubeny et al. (2005) suggests the use of separate values of a and b for shallow (z/D < 0.5) and deep (z/D > 0.5) embedment, and for smooth and rough pipes.

Equation 2.4 can be rewritten in the form shown in Equation 2.5. The fitting parameters a and b assume values of 6 and 0.25, respectively (Randolph and White, 2008).

$$\frac{V}{S_u D} = a\left(\frac{z}{D}\right)^b \quad \text{(Eq. 2.5)}$$

In very soft sediments, specially soils that are in the remolded state (soft clays of sands that undergone liquefaction) the contribution of the buoyance resistance must be included in Equation 2.4 (Randolph and Gourvenec, 2011). The pipeline embedment can be estimated by Equation 2.5(Simpson et al. 2015). Westgate (2009) suggests that the S_u used in Eq. 2.6 should be $S_{u,rem}$ due to soil disturbance as loss of strength caused by the dynamic movement of the pipeline during the laying process.

$$\frac{V}{S_u D} = \min\left[6\left(\frac{z}{D}\right)^{0.25}; 3.4\left(\frac{10z}{D}\right)^{0.5}\right] + 1.5\frac{\gamma' A_{bm}}{D S_u} \quad \text{(Eq. 2.6)}$$

Where γ' is the soil submerged unit weight and A_{bm} is the pipe submerged cross-sectional area, which can be calculated by:

$$A_{bm} = \frac{D^2}{4}(\beta - sin\beta cos\beta) \leq \frac{\pi D^2}{4} \quad \text{(Eq. 2.7)}$$

$$\beta = cos^{-1}\left(1 - \frac{2z}{D}\right) \quad \text{(Eq. 2.8)}$$

Where β is the enclosed angle (in radians). If z/D > 1, β = π. A schematic illustration of the pipe cross-section area submerged in the seabed soil is shown in Figure 2.6.

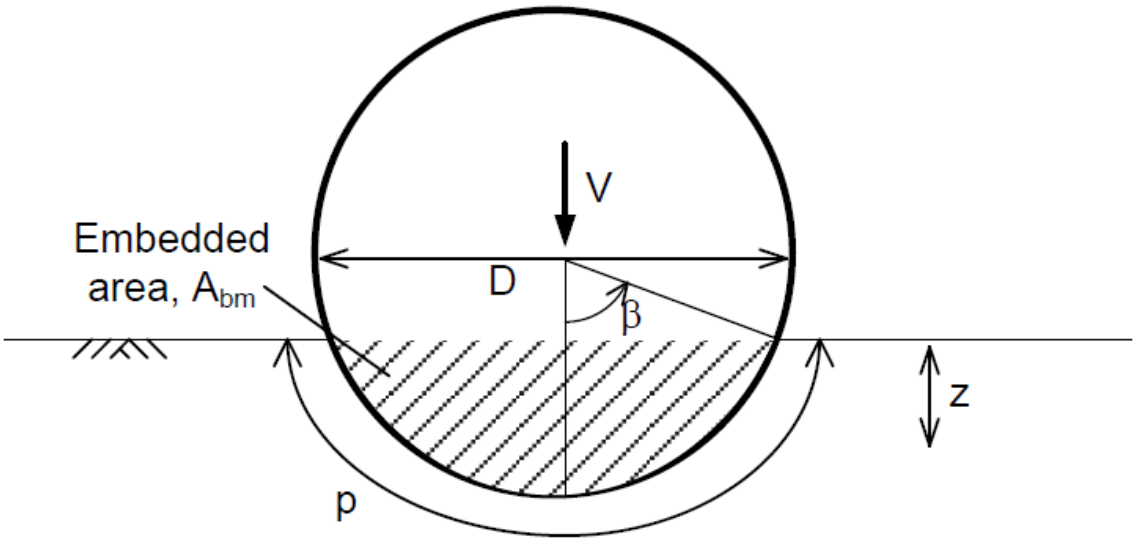

Figure 2.6. Pipe cross-section area submerged in seabed soil (Simpson et al., 2015).

A touchdown lay factor (k_{lay}) can be used to account for the vertical force concentration and dynamic motion in the touchdown zone during the laying process (Randolph and White, 2008):

$$k_{lay} = 0.6 + 0.4\left(\frac{EIk_{lay}W_i}{z_{ini}{T_0}^2}\right)^{0.25} \geq 1 \qquad \text{(Eq. 2.9)}$$

Where $k_{lay} = V/W_i$, EI is the pipeline bending stiffness, W_i is the submerged pipe weight during installation, z_{ini} is the initial pipe embedment immediately after laying, and T_0 is the horizontal component of the effective lay tension in the pipe at the touchdown point during installation. Typical values of k_{lay} vary from 1 to 3. Equation 2.9 is only valid for:

$$T_0 > [3(EI)^{0.5}W_i]^{\frac{2}{3}} \qquad \text{(Eq. 2.10)}$$

2.6 CONSOLIDATION AFTER LAYING

After the initial penetration of the pipeline, further settlement occurs due to consolidation of the soil beneath the pipe. When the pipeline is laid on the seabed, excess pore pressure is generated and the effective stresses beneath the pipe remain the soil. As time progress, the excess pore pressure is dissipated, the soil consolidates and the effective stresses at the pipe-soil interface increase. This process can be compared to the "set-up" of piles driven in clay. The consolidation time can be simply estimated based on elastic calculations for 1-D consolidation (Eq. 2.11). Krost et al. (2010) recommends using the full pipe diameter instead of the chord length (part that is embedded) when estimating the consolidation time. For soft sediments, the time to achieve a degree of consolidation of 90% (U_{90}) can take more than 1 year depending on the pipe embedment and the coefficient of consolidation (c_v) of the soil. The time-scale of consolidation is relevant for estimating the axial resistance at the pipe-soil interface during axial and lateral movements. (Randolph and Gourvenec, 2011; White and Randolph, 2007).

$$T = \frac{c_v t}{D^2} \qquad \text{(Eq. 2.11)}$$

2.7 DRAINED RESIDUAL SHEAR STRENGTH AT THE INTERFACE BETWEEN SOILS AND SOLID INTERFACES

Tika-Vassilikos (1991) performed tests using a ring shear apparatus to study the effect of rate of shearing on the shear resistance between soil and steel at large displacements. The tests were conducted at an effective normal stress of 9400 psf (450 kPa). The steel used in the tests had an average roughness of about 8.5 μm. The clay used in the tests had a liquid limit of 71%, plastic limit of 26% and a clay fraction of 53%. The thickness of the soil specimens used in the tests were 0.49 in (12.5 mm) and 0.75 in (19

mm) in the clay interface and the clay tests, respectively. The water content of the clay before shearing was about 30.5%. A faster shear rate was used prior to slow rates (drained shearing) so the residual strength could be measured. Residual conditions were reached at displacements of about 1.18 in (30mm). The drained residual interface angle was equal to 9^{o}. The residual interface efficiency, which is the ratio of the residual interface strength and the clay residual strength, was equal to 0.82.

Lehane and Jardine (1992) carried out tests in a ring shear device to measure the drained residual at the interface between stainless steel and Bothkennar clay. The clay used in the tests had a liquid limit of 80%, a plastic limit of 32% and a clay fraction of 35%. The effective normal stresses used in the tests ranged from 1045 to 2715 psf (50 to 130 kPa). A slow shearing rate (0.0003 in/min or 0.008 mm/min) was used in order to simulate drained loading conditions. For tests conducted at an effective stress of 1045 psf, residual conditions were mobilized at a displacement of 1.97 in (50 mm) and the residual friction angle at the interface ranged from 30^{o} to 32^{o}. The specimens were visually inspected after failure had occurred and it was noted that the slip occurred within the soil.

Tsubakihara et al. (1993a,b) used a direct shear device to study the shear strength at the interface between normally consolidated clay and steel. The clay used in the tests was Kawasaki marine clay, which had a plasticity index of 48% and a clay fraction of about 60%. The thickness of the remolded soil specimen was about 0.55 in (14 mm) and an effective normal stress of 6140 psf (294 kPa) was used in the tests. The specimens were sheared at slow rate (0.001 in/min or 0.03 mm/min) so that drained conditions could be achieved. Secant friction angles of ranging from 19^{o} to 24^{o} were measured under those conditions. When the steel roughness was increased from 2 to 7 μm, the residual interface efficiency increased from 72 to 90%. Additionally, when the steel roughness was increased from 3 to 30 μm, the residual secant interface friction angle increased from 20^{o} to 28^{o}, for

the soil a secant friction angle of 27º was measured. The specimens were only mobilized to a maximum displacement of 0.6 in (15 mm).

Lemos and Vaughan (2000) measured the residual interface shear strength between six different soils and three different interfaces materials of varying roughness by using a ring shear device. The soil specimens were tested in the remolded state. Effective normal stresses ranging from 2088 to 10443 psf (100 to 500 kPa) were used in the tests. Residual conditions were achieved after a few centimeters of displacement. The residual secant friction angles of the clays ranged from 15º to 28º. Values of residual interface efficiencies were reported to increase from 60 to 85%, as the surface roughness of the solid interfaces increased from 1 to 10 µm. Additional direct reversal shear tests were conducted to measure the residual interface strength between kaolinite, which had a plastic index of 36% and a clay fraction of 82%, and a smooth interface with a mean CLA of 0.22 µm. A shear rate of 0.0013 in/min (0.0337 mm/min) was used to simulate drained loading conditions, and an effective normal stress of 4177 psf (200 kPa) was used. The results indicated a residual secant interface friction angle of about 10º. Residual condition was achieved at displacements of about 0.39 in (10mm).

Direct shear and torsional ring shear devices are conventional laboratory devices used to measure the residual shear strength at the interface between soils and solid interfaces. However, most of the tests performed for this purpose in these devices involve applying a normal stress greater than 313 psf (15 kPa) and usually ranging from 1044 to 20,885 psf (50 to 1,000 kPa), which may not be representative of the very low effective normal stresses applied on subsea flowlines. Additionally, for that stress range, the applied shear stresses are very small and the friction in the mechanical device may significantly influence the measurements (Fang et al. 2004). These devices were extensively used to measure the residual interface shear strength between clays and polymeric geosynthetics

(Byrne et al. 1992; Stark and Poeppel 1994; Gilbert and Byrne 1996; Merril and O'Brien 1997; Fox and Stark 2004; and Gilbert et al. 2004). Residual interface efficiencies were reported to be as low as 35% for interfaces between smooth geomembrane and clay, and values as high as 100% were reported for textured geomembrane. In general, the displacement required to mobilize residual strengths ranged from 1.97 to 3.94 in (50 to 100 mm). However, for thinner specimens (about 0.02 to 0.06 in), displacement values of 0.2 to 0.4 in were reported by Gilbert et al. (2004). Chandler and Hardie performed tests using London clay and concluded that the displacement required to reach residual conditions decreases as the specimen thickness decreases.

For tests where very low effective normal stresses must be applied, tilt-table tests may be an alternative to conventional laboratory tests. It has the advantage of eliminating the machine friction, which can significantly influence the tests results, not forcing failure to occur along the interface and very low stresses can be applied since surcharge weights applied on a loading plate on top of the specimen. However, displacements cannot be controlled, post-peak response cannot be measured, the stress applied on the specimen depends on surcharge weight, which may topple, loading eccentricity may influence the results since the applied stress becomes non-uniform as the table is tilted (Pederson et al. 2003). Liu et al. (1997) performed tilt-table tests on bentonite and geomembrane applying an effective normal stress of 1 kPa and measured a drained secant friction angle of 24^0 for the peak shear strength at the interface between the two materials. Pederson et al. (2003) conducted tilt-table tests using kaolinite and two different solid interfaces (acrylic and anodized aluminum) and applying effective normal stresses ranging from 2.1 to 42 psf (0.1 to 2 kPa). For a stress level of 42 psf, values of interface efficiencies (in terms of peak shear strengths) of 80% for the anodized aluminum and 90% for the acrylic. Najjar et al. (2003 and 2007) performed tilt-table tests on Gulf of Mexico clay obtained from two

different locations and four different solid interfaces applying effective normal stresses lower than 104 psf (5 kPa). Plasticity index and liquid limit values for the two clays were reported as 35%, 40% and 120%, 98%, respectively. The thickness of the soil specimens was about 0.06 in. For the clay with higher plasticity index, it was residual interface secant friction angles ranging from 23^{o} to 39^{o} while for the clay it was measured values ranging from 27^{o} to 37^{o}. The displacements mobilized to reach residual conditions ranged from 0.98 in to 1.97 in (25 to 50 mm). The reported Mohr-Coulomb failure envelopes for the drained residual interface strength were curved at very low effective normal stresses, becoming flatter as the effective normal stress increase. They concluded that the drained residual interface strength between the clay and the solid interface depends on both the composition of the clay and the material and roughness of the interface, which is consistent with results obtained by Bae (2009).

Chapter 3: Gulf of Mexico Clay Set-up Time Based on T-bar Tests

3.1 Introduction and Objectives

The objective of this chapter is to describe how the set-up time of Gulf of Mexico clay can be estimated by performing T-bar tests. The increase in the undrained shear strength (S_u) of the clay is measured as a function of time, having as primary goal to obtain the time required for the rate of increase in Su to be considered small enough for practical purposes in future lab tests. Additionally, the remolded shear strength ($S_{u,r}$) is compared to the value obtained from T-bar tests performed at different time intervals after remolding the soil.

3.2 Gulf of Mexico Clay

The soil used in this study is a marine clay obtained directly from the Gulf of Mexico. The soil index properties of the Gulf of Mexico clay are shown in Table .

Table 3.1 Soil Index of Gulf of Mexico Clay (Gerkus, 2016)

Liquid limit (%)	105
Plasticity limit (%)	62
Specific gravity	2.75

3.3 Soil Test Bed

The soil was placed as a single layer into a 4x2x2 ft thermoplastic tank (Figure 3.1) and mixed with saline water with a target water content ranging from 120-130%, which is representative of in-situ water contents for Gulf of Mexico clay. Since the tank is relatively small, the water content variation within the tank was found to be very small, with changes no greater than 5%. A paint mixer (Figure 3.2) was used to mix the soil with saline water with 35 grams of sea salt per liter of fresh water, which is representative of the salt

concentration in the sea water. The torque capacity of the drill is 900 rounds per minute, making it capable of reconstituting the soil with S_u ranging from 0 to 90 psf, approximately. The mixer has a 28-in long rod and 12-in wide steel paddle. The paddle with slightly bended horizontal components helps to displace the soil when mixing.

Figure 3.1 Soil Test Bed.

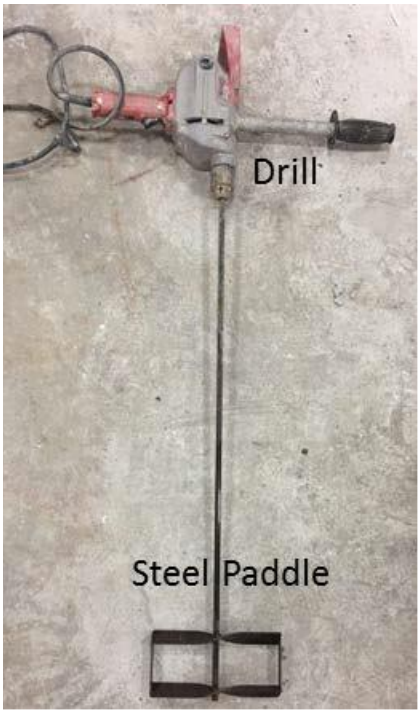

Figure 3.2 Soil Mixer

3.4 T-BAR TEST APPARATUS AND PROCEDURE

The T-bar penetrometer was used to measure the undrained shear strength of the soil test bed. It consists of a short cylindrical bar that is 4-in long and 1-in in diameter which is attached at right angles to a penetrometer rod (Figure 3.3). The T-bar is inserted into the soil by pushing the rod at a constant rate of 0.8 in/s (20 mm/s) with the aid of weights attached on top of the penetrometer rod. A load cell attached to the top of the rod measures the differential force, also called net pressure, on the bar. A separate penetration test is conducted at the same spot by removing the acrylic rod (T-bar) and only measuring the differential force due to the friction and the bearing resistance of the penetration rod. In order to better capture the S_u of the soil and/or to measure the remold undrained shear strength ($S_{u,r}$), usually three T-bar penetrometers tests are conducted at the same spot, followed by the test without the acrylic rod.

The measured net pressure is related to the undrained shear strength of the soil by a plasticity solution (Eq. 3.1):

$$s_u = \frac{(F_{total} - F_{rod})}{N_c * A} \quad \text{(Eq. 3.1)}$$

Where:

F_{total} = the total measured resistance during the T-bar insertion

F_{rod} = the measured resistance when only the rod is inserted into the soil

A = the projected area of the T-bar

N_c = bearing capacity factor

N_c can be assumed as a constant value of 10.5 (Stewart and Randolph, 1994), but for shallow depths, it should be corrected due to the variation in resistance from soil strength and soil buoyance. For lab applications, the depth at which N_c should be adjusted can go up to 7.5-15D, where D is the diameter of the T-bar (White et al. 2010). For this series of testing, N_c was corrected up to a depth of 2.5D. For the upper 2.5D of penetration, N_c was linearly interpolated between $N_c = 5$ at the surface and $N_c = 10.5$ at 2.5D. An example of the change in N_c for a depth of 15 in is shown in Figure 3.4.

The geometric characteristics and the parameters considered in the calculations for the T-bar used in the tests are shown in Table 3.2.

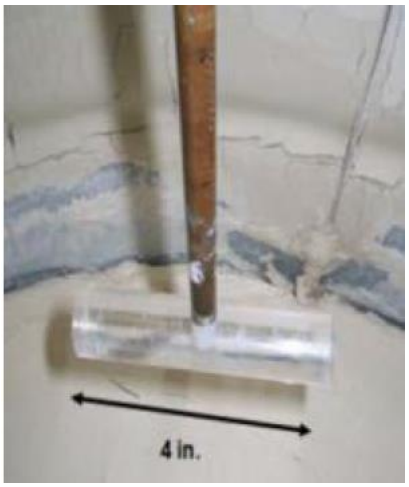

Figure 3.3 Acrylic T-bar and Penetrometer Rod (Gilbert et al. 2012)

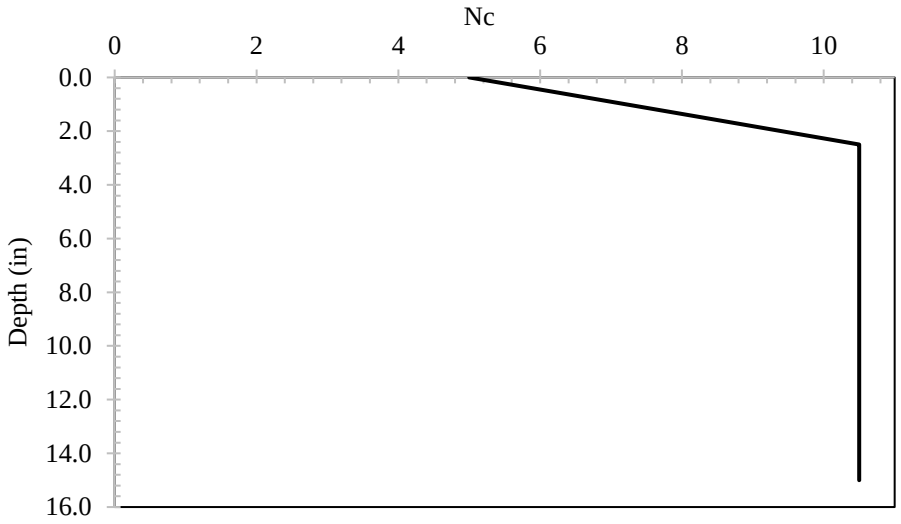

Figure 3.4 Example of the change in N_c as a function of depth.

Table 3.2 T-bar Information

Diameter (in)	1
Area (in^2)	4
N_c	10.5
N_c correction depth (in)	2.5

3.5 Load Frame

The load frame (Figure 3.5) is essentially comprised of an aluminum load frame with an extended wooden arm and rests on top of a steel tank. This load frame was originally built by Lee (2008) but a few alterations were made so that it would accommodate the new set of pulleys and also fit into the available space in the lab. The loading system works as follows: a plastic wire is attached to an electric motor on one side of the load frame; this wire pass around the load frame with the help of four pulleys that are installed along the load frame, thereby reaching the other end (extended wooden arm) where the last pulley makes it go downwards; this is where the wire is attached to load cell followed by the T-bar.

Figure 3.5 Load Frame

3.6 ELECTRIC MOTOR

A stepper motor (powered by a Super Electric SLO-SYN MH112-ff-206) was used to apply a constant displacement rate to the loading lines (Figure 3.6). The motor is located on the right side of the load frame (opposite to the extended wooden arm) and rests on top

of an aluminum plate. The motor can supply a maximum loading rate of 50 RPS (round per second), which corresponds to approximately 18.9 in/s for line displacement (Figure 3.7).

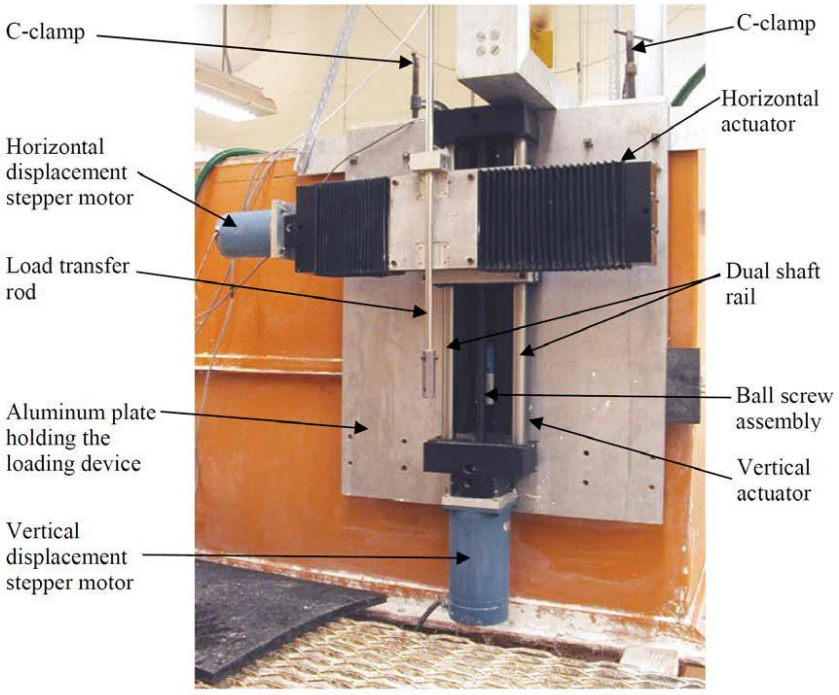

Figure 3.6 Stepper Motor (Huang, 2015)

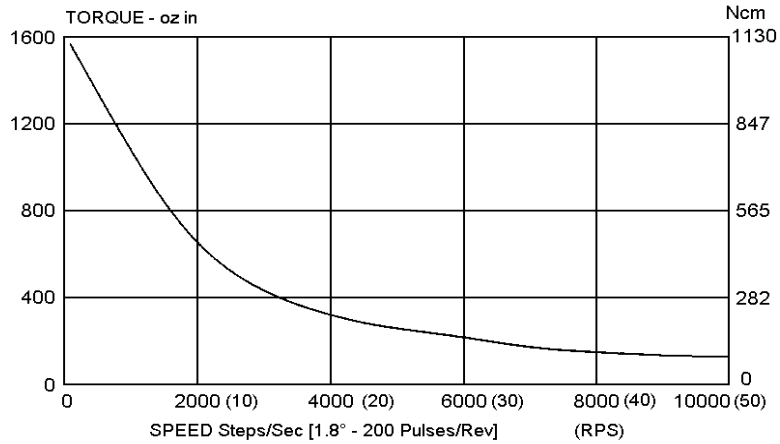

Figure 3.7 Torque versus Speed Curve of Stepper Motor (Lai 2017)

3.7 LOAD CELL

A load cell manufactured by Lebow Products Inc. (Figure 3.8) with maximum capacity of 200lbs was used to measure the loads during testing. The compressive and tensile loads result in a positive and negative voltage output, respectively. The load in pounds can be calculated by subtracting a zero-voltage reading from the output and multiplying the result by a calibration factor, obtained from calibration tests (Huang, 2015).

Figure 3.8 Load cell (Huang, 2015)

3.8 LINEAR MOTION TRANSDUCER

The linear motion transducer (LMT) is a RayecoTM model P-50 and can record displacements up to 50 in. The LMT was attached to a track system on the aluminum load frame (Figure 3.9). It was calibrated by placing a steel tape measure next to the track system and the displacement of the LMT sensor was observed and recorded. A plastic wire was used to attach the LMT to the loading system, the friction due to the plastic wire was found to be negligible for this test.

Figure 3.9 Linear motion transducer

3.9 DATA ACQUISITION AND MOTION CONTROL PROGRAMS

The data acquisition and motion control system were developed by Huang (2015) on LabVIEW platform, which records data from the Data Acquisition (DAQ) hardware (Figure 3.10) and motion control card, both manufactured by National Instruments. The DAQ program records data obtained from the load cell and the LMT with respect to time and saves it in text file format. The DAQ program interface area (Figure 3.11) is comprised of a controlling panel, which allows the user to start and stop recording data and write and save text files, and a calibration area, which allows the user to input calibration factors (convert voltage signals from load cell, LMT and LVDT into real load and displacements). Additionally, the output of loads and displacements with respect to time are updated in real time as testing progress and can be seen on the right side of the interface.

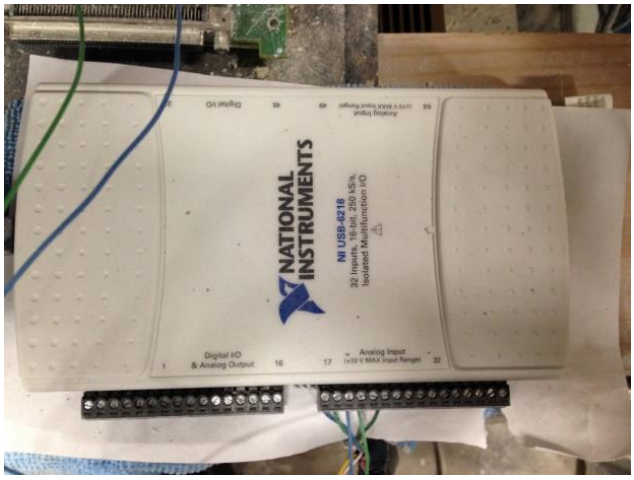

Figure 3.10 Data Acquisition Hardware

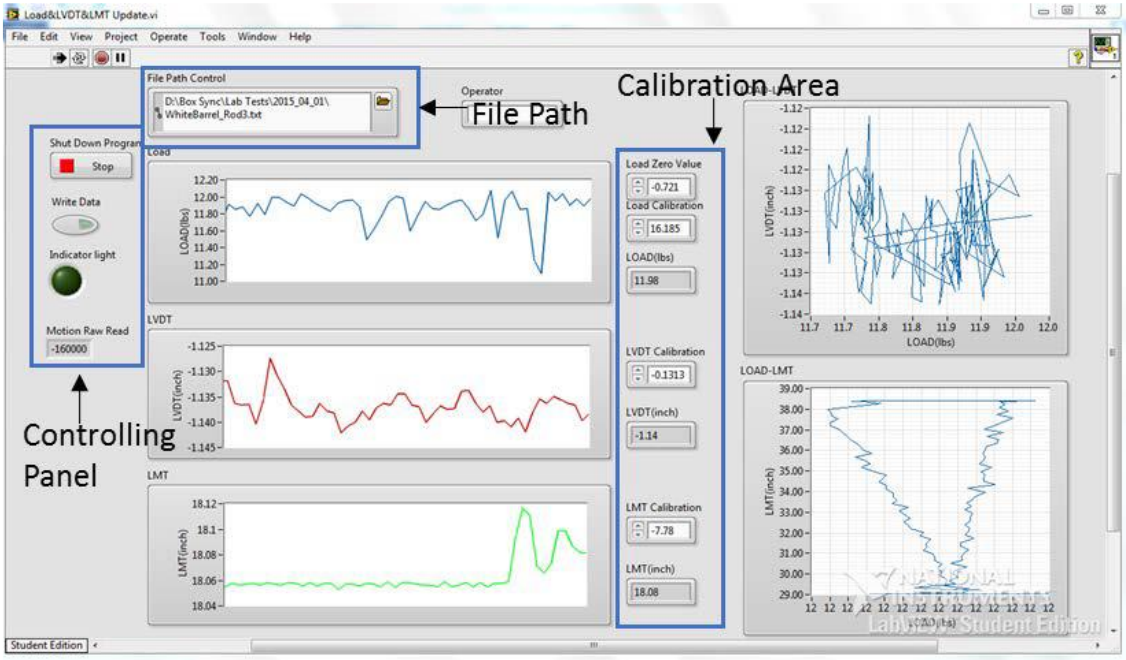

Figure 3.11 LabVIEW User Interface (Huang, 2015)

3.10 TEST PROGRAM

Three groups of tests were performed to analyze the increase of the undrained shear strength of the Gulf of Mexico clay as a function of time. They are summarized in Table

3.3, 3.Table , and 3.Table 3.5. The time interval column in the tables below corresponds to the time that the T-bar was conducted after mixing the clay.

Table 3.3 Tests in Group A

Test number	Time interval (hr)	Water content (%)
1A	0.17	127
2A	1.25	127
3A	4.60	127
4A	31	125
5A	72	Not available
6A	144	Not available
7A	240	124

Table 3.4 Tests in Group B

Test number	Time interval (hr)	Water content (%)
1B	0.33	125
2B	24	124
3B	72	Not available
4B	100	124

Table 3.5 Tests in Group C

Test number	Time interval (hr)	Water content (%)
1C	0.17	Not available
2C	24	140

3.11 RESULTS

The T-bar curves (S_u versus depth) for all the tests in Group A, B, and C are shown in the Appendix A. The summary of the results for Groups A, B and C are shown in Table 3.6, 3.7 and 3.8, respectively. Figure 3.12 shows the increase in the undrained shear strength as a function of time. Studies conducted by Norena (2015) indicates that if the results obtained from the 3rd and the 10th T-bar cycle are normalized by the measurement

from the 1st cycle, the difference between them is very small, thus, for this study, the measurements from the 3rd T-bar cycle were assumed to be representative of the remolded shear strength of the clay. The undrained shear strength obtained from the 3rd T-bar cycle test is shown in Figure 3.13 as a function of time. The measured sensitivity between the 1st T-bar cycle and the remolded undrained shear for each group is plotted with time in Figure 3.14.

Table 3.6 Summary of tests in Group A

Test number	**Time interval (hr)**	**S_u (psf)**	**$S_{u,R}$(psf)**	**S_u / $S_{u,R}$**
1A	0.17	1.5	1.4	1.1
2A	1.25	1.5	1.4	1.1
3A	4.60	1.7	1.4	1.3
4A	31	3.0	T-bar 3 not measured	T-bar 3 not measured
5A	72	3.2	1.8	1.8
6A	144	3.2	T-bar 3 not measured	T-bar 3 not measured
7A	240	4.1	1.8	2.3

Table 3.7 Summary of tests in Group B

Test number	**Time interval (hr)**	**S_u (psf)**	**$S_{u,R}$(psf)**	**S_u / $S_{u,R}$**
1B	0.33	2.2	1.8	1.2
2B	24	3.3	1.8	1.8
3B	72	3.8	T-bar 3 not measured	T-bar 3 not measured
4B	100	3.8	1.9	2.1

Table 3.8 Summary of tests in Group C

Test number	**Time interval (hr)**	**S_u (psf)**	**$S_{u,R}$(psf)**	**S_u / $S_{u,R}$**
1B	0.33	1.2	1.0	1.2
2B	24	3.1	1.2	2.6

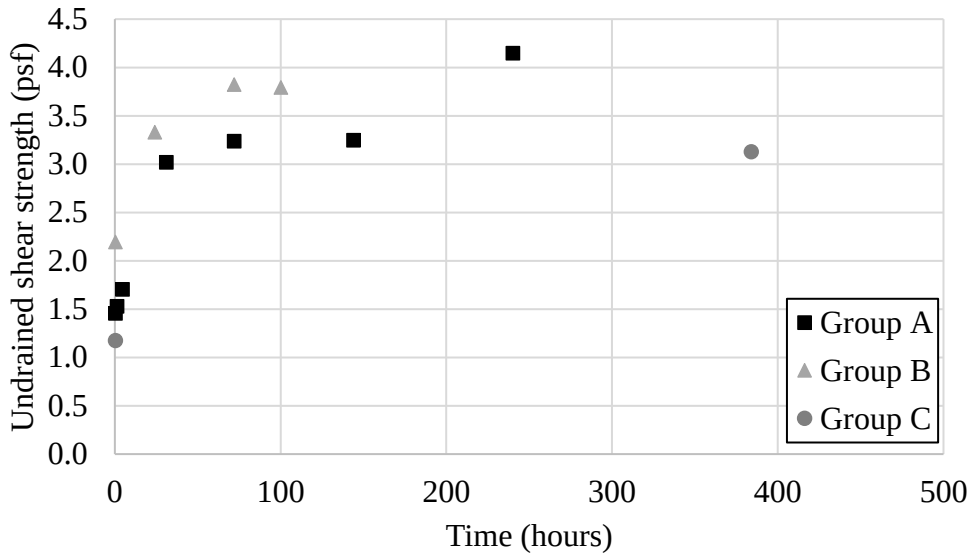

Figure 3.12 Undrained shear strength as a function of time

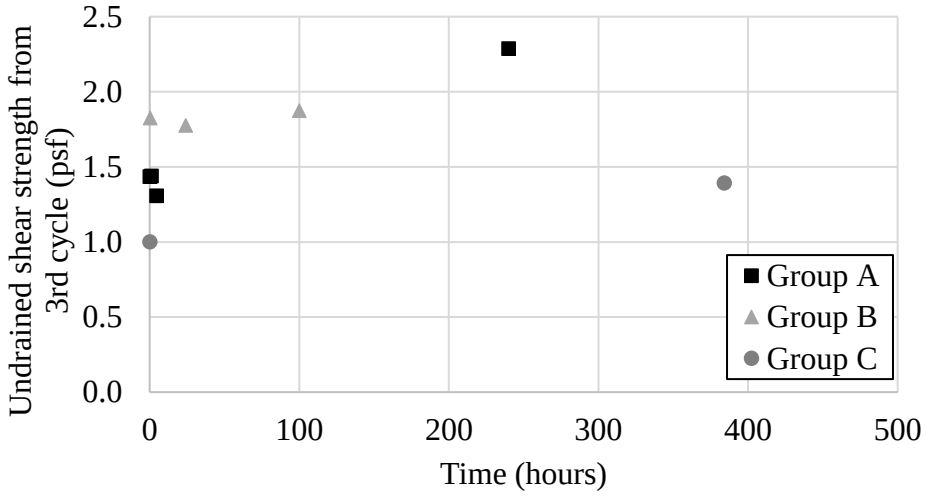

Figure 3.13 Undrained shear strength from 3rd T-bar cycle as a function of time

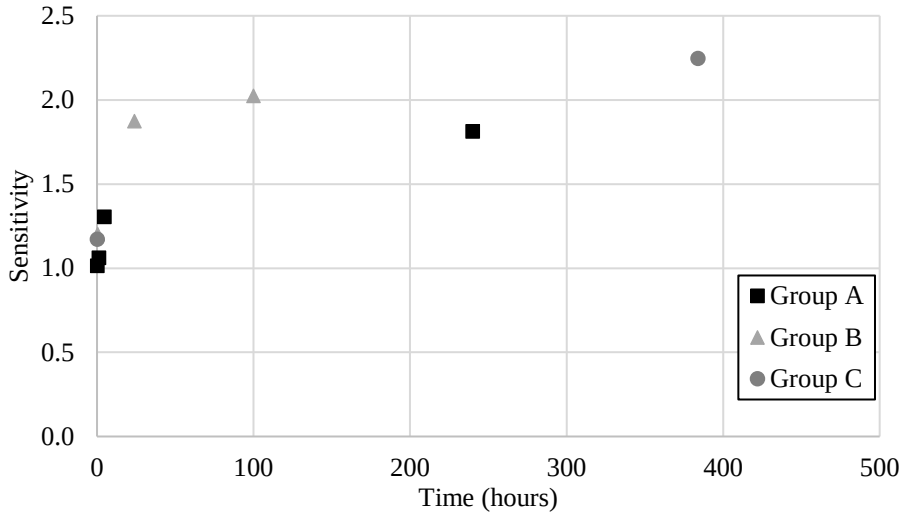

Figure 3.14 Sensitivity (between 1st and 3rd T-bar cycle) as a function of time

3.12 DISCUSSION

The index properties of the soil used in this study is within the range of values presented in the literature based on in-situ samples obtained from shallow depths (Table 3.9). The liquid limit (LL) and plasticity index (PI) can significantly vary due to the different clay mineralogy encountered in different sites in the Gulf of Mexico.

Based on Tables 3.3 and 3.4, the water content remains relatively constant within the time interval considered in this study. Thus, the increase in S_u can be explained a phenomenon known as thixotropy, which can be defined as an isothermal, reversible and time-dependent increase in undrained shear strength without any change in volume or void ratio (at a constant water content). In other words, after remolded, the interparticle cohesive bonds will rearrange themselves with time, causing an increase in the undrained shear strength.

Table 3.9 Comparison of index properties of Gulf of Mexico clay

Author	LL (%)	PI (%)	Gs	WC (%)
Jean et al. (1998)	-	65-100	-	90-150
Francisca et al. (2005)	102	57	-	-
	72	42	-	-
	55	27	-	-
Najjar et al. (2007)	116-123	82-87	-	150
	95-102	57-62	-	120
	86-98	55-60	-	115-133
	86-89	55-60	-	86-93
	68	42	-	50
Low et al. (2010)	-	18-112	-	32-62
Murali and Biscontin (2014)	97	37	2.74	135
	99	35		130
	102	37		132
Taukoor et al. (2018)	82	50	2.68	84
Taukoor et al. (2019)	88	52	-	92-95

From the T-bar test results, S_u remains close to the remolded value for the first 1.25 hours. After about 4.5 hours, S_u seems to increase. After about 72 hours, no significant increase in S_u was observed, except for test 7A.

Additional tests are not included in Figure 3.13 and Figure 3.14 because measurements of the 3rd cycle of the T-bar were not available. It can be inferred from Figure 3.13 that the S_u obtained from the 3rd cycle of the T-bar remains constant for the first 5 hours and assumes a value similar to the one obtained right after mixing the clay ($S_{u,r}$). As can be seen in Figure 3.14, the sensitivity of the clay increases with time as both S_u and $S_{u,R}$ increase.

For the short time interval used in this study, the values of sensitivity ranged from 1.8 to 2.6, which is consistent with values presented in the literature for Gulf of Mexico clay (Table 3.10). The values in Table 3.10 were obtained based on field tests and high-quality samples recovered from the field.

The sensitivity of the clay seems to not significantly vary with depth for strengths profiles obtained after remolding the soil and after "set-up" has occurred. As an example, the sensitivity profile for test 1A and 5A are shown in Figure 3.15 and 3.16, respectively. For test 1A, which was conducted within a few minutes after remolding the soil, the sensitivity seems remain relatively constant as depth increases, which was expected since the soil still very close to the fully remolded state. For test 5A, the sensitivity slightly decreases as depth increases, assuming a value of approximately 1.8 at a depth of 2.5 in and 1.7 at a depth of 10 in, which is due to the increase in effective normal stress as depth increases, causing more resistance from the clay particles when subjected to multiple T-bar cycles. For the purpose of this study, this change in the sensitivity as a function of depth can be neglected. The sensitivity values for very shallow depths (up to 1 in) are not shown in Figure 3.16 due to considerable variation mostly due to the very low effective stresses and the change in the bearing factor.

Besides the tests included in Group A, B and C, additional tests were conducted within 4 hours after remolding the clay. A relationship between remolded undrained shear strength and initial water content can be obtained from the test results using a best fit polynomial function and it is shown in Figure 3.17. As can be seen in the figure below, the initial water content significantly influences $S_{u,r}$ shortly after remolding the soil. For instance, a decrease in about 20% in water content can cause an increase in $S_{u,r}$ of approximately 300%. This relationship can be plotted as a linear function by presenting the y-axis in log scale (Figure 3.18).

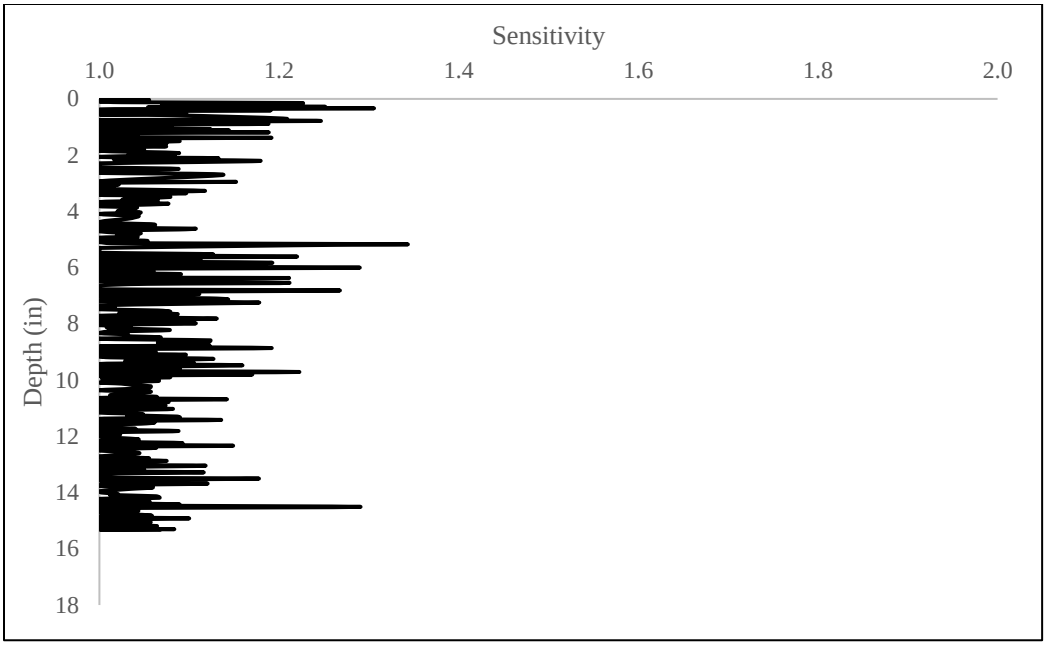

Figure 3.15 Sensitivity profile for test 1A

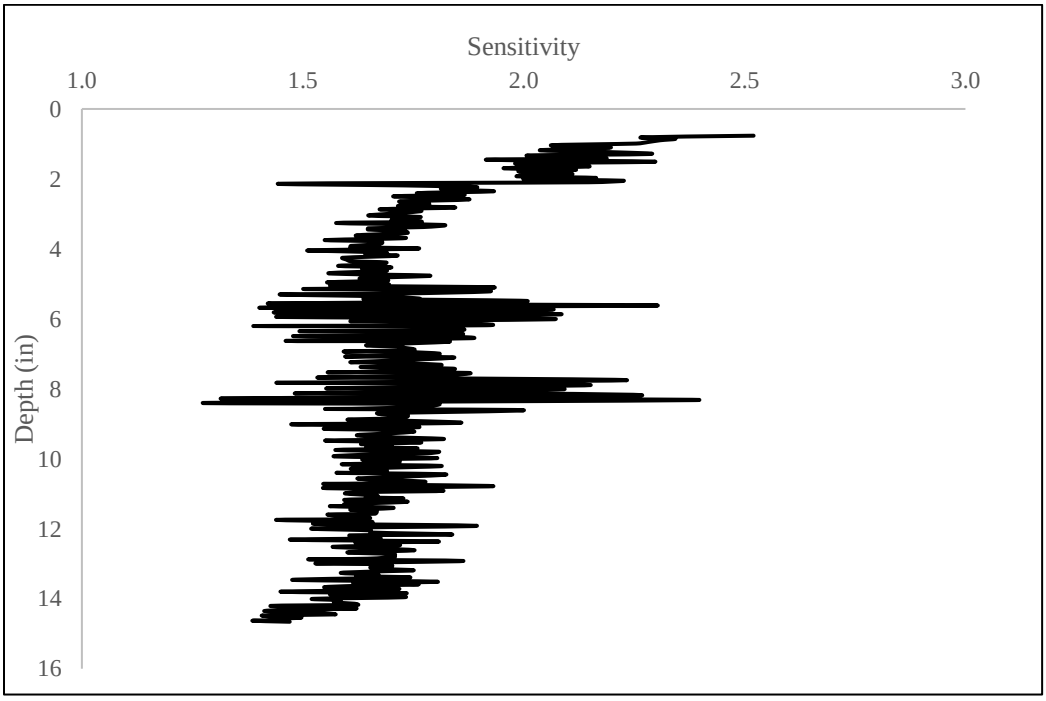

Figure 3.16 Sensitivity profile for test 5A

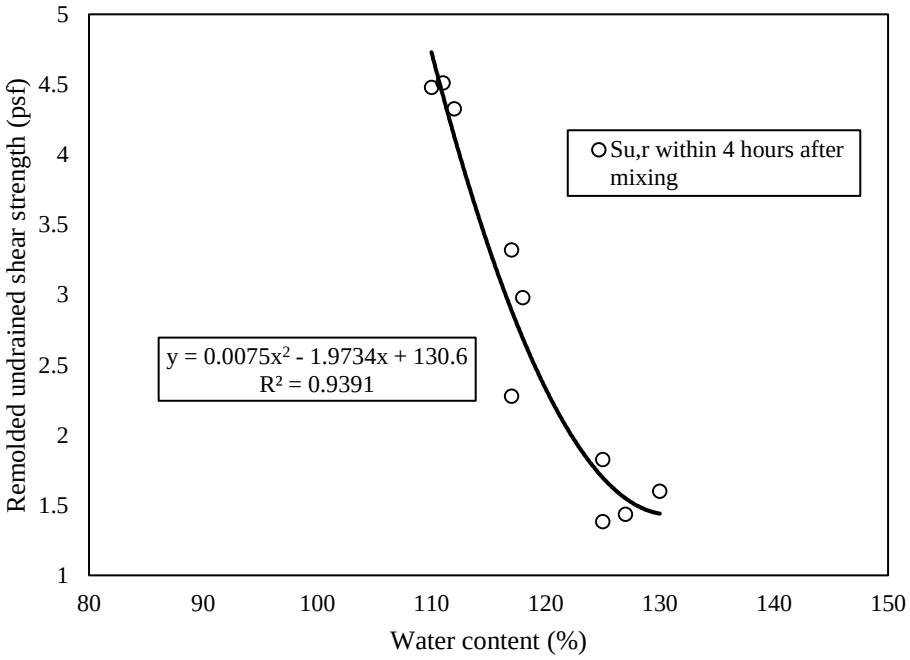

Figure 3.17 Relationship between $S_{u,r}$ and water content shortly after remolding the soil

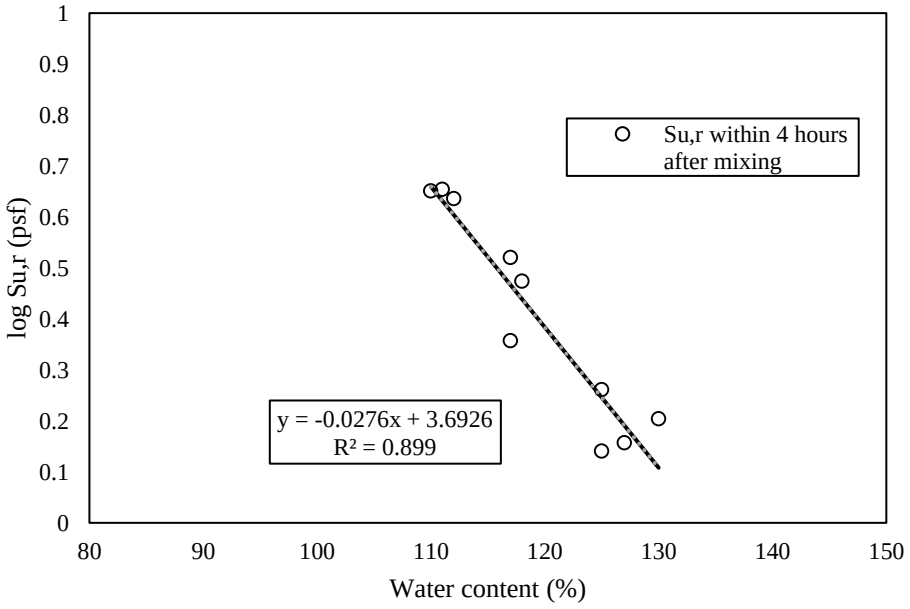

Figure 3.18 Relationship between log ($S_{u,r}$) and water content shortly after remolding the soil

Table 3.10 Comparison of sensitivity values of Gulf of Mexico clay

Source	Sensitivity	Test	Depth (ft)
Low et al. (2010)	1.1 to 7.6	Vane Shear, Fall Cone	Not Available
Taukoor and Rutherford (2016)	2 to 4	Vane Shear and T-bar	0 to 2.6
FUGRO (2005)	1-2	Miniature Vane Shear	0 to 33

3.12 CONCLUSIONS

In this study, T-bar tests were used to measure the increase in S_u as a function of time for Gulf of Mexico clay, focusing on short periods of time for laboratory applications. Three sets of T-bar tests were analyzed, and the following conclusions can be drawn:

1. The results indicate that, since the water content remains approximately the same as time elapses, and the increase in S_u is due to thixotropy of the clay. Thixotropy has an impact on the S_u shortly after the clay has been mixed (remolded state). This impact became less noticeable after 72 hours, suggesting that within 3 days after mixing, a large portion of the increase in S_u due to thixotropy has occurred.
2. The results also indicate that S_u rapidly increases during the first hours after mixing the clay, assuming a value that is approximately two times greater than the remolded value after 72 hours. Based on the tests in Group A, further studies need to be conducted in order to confirm if S_u still significantly increasing within 10 days after the clay has been mixed.
3. The sensitivity values of Gulf of Mexico are consistent with values obtained in the literature using both laboratory and field tests.
4. An empirical correlation is proposed to estimate the remolded undrained shear strength shortly after the clay is remolded based on the initial water content. This

relationship indicates that a decrease in about 20% in water content can cause an increase in $S_{u,r}$ of approximately 300%.

5. For tests conducted shortly after remolding the soil, the sensitivity does not seem to change as depth increases. However, for tests conducted after "set-up" of the clay has occurred (after 72 hours), the sensitivity seems to slightly decrease as depth increases, which is may be due to the increase in effective normal stress, causing more resistance from the clay particles when subjected to multiple T-bar cycles.

Chapter 4: Pipe Embedment Tests in Gulf of Mexico Clay

4.1 Introduction and Objectives

The objective of this chapter is to present the studies conducted to measure the embedment depth of a pipe made of polypropylene in Gulf of Mexico clay. The primary focus of the testing was to compare the results with the prediction method outlined Simpson et al. (2015) for initial embedment and to estimate the pipe settlement and consolidation rate after initial embedment. The Gulf of Mexico clay as well as the loading system used in these tests are the same ones used in the tests discussed in Chapter 3.

4.2 Soil Test Beds

The preparation procedure of the soil test beds is similar to the one described in Chapter 3. For these tests, two thermoplastic tanks were used: a small tank 4x2x2 ft (same tank used for the tests discussed in Chapter 3) and a large tank (46 x 36 x 24in) (Figure 4.1).

Figure 4.1 Large tank.

4.3 TEST PROGRAM

A total of 9 tests were performed with a 3, 10, 6, and 9-ft long sections of a polypropylene pipe. For the tests performed with the 3-ft long section, the clay surface was covered with a 1 to 2 in layer of tap water. For the other tests, the pipes were fully submerged. The remolded undrained shear strength ($S_{u,r}$ from T-bar test), the water content (w), the water level (z_w), the submerged unit weight of the pipe (V), the drop rate of the pipe, and the duration of the test are provided in Table 4.1. For the hand-placed pipes, the duration corresponds to the elapsed time after the pipe was placed. However, measurement of the data was only possible after several minutes (up to 180 min).

Additionally, the T-bar results were corrected up to a depth of 2.5D and the $S_{u,r}$ was obtained from the 3rd T-bar penetration conducted at a chosen location near the pipe.

Table 4.1 Summary of tests

Test No.	**Pipe length (ft)**	**$s_{u,R}$ (psf)**	**w (%)**	**z_w (in)**	**V (lb/ft)**	**Drop rate (in/s)**	**Duration (hrs)**
1	3	1.9	125	1 to 2	4.1 to 4.9	0.8	0.33
2	3	1.4	125	1 to 2	3.7 to 4.4	0.8	0.29
3	3	2.0	128	1 to 2	4.2 to 5.0	0.8	0.28
4	10	1.5	142	Submerged	6.01	Hand-placed	0.5
5	10	1.3	140	Submerged	4.05	Hand-placed	0.4
6	6	1.4	130	Submerged	2.8	Hand-placed	300
7	9	1.4	130	Submerged	2.8	Hand-placed	300
8	6	2.5	107	Submerged	6.0	Hand-placed	335
9	9	2.5	107	Submerged	6.0	Hand-placed	335

4.4 TEST PROCEDURE

T-bar tests were performed before conducting the embedment tests in order to obtain S_u and $S_{u,r}$. Details about how a T-bar is performed can be found in Chapter 3.

4.4.1 SMALL TANK, 3 FT LONG PIPE

The clay was mixed and left to set-up for approximately 48 hours and a water content measurement was taken.

The 3-ft long pipe was filled with commercial sand to achieve the desired V and both ends were sealed to avoid water getting inside the pipe and changing the value of V. The total weight of the pipe per linear foot is 9.33 lb/ft and the outer diameter of the pipe (OD) is 4.25 in. The 3-ft long pipe is shown in Figure 4.2.

Figure 4.2 3-ft long pipe section being lowered into GoM clay.

The pipe was lowered at a rate of 0.8 in/s into the clay using the same load frame and motor used for the T-bar tests. The embedment was measured using a linear motion transducer (LMT) that runs along the top of the load frame. Details about the loading system and the LMT can be found in Chapter 3.

4.4.2 LARGE TANK, 6 FT, 9 FT AND 10 FT LONG PIPES

As with the embedment tests conducted in the small tank, the clay was mixed and left to set-up for at least 72 hours and a water content measurement was taken.

Commercially available #3 rebars were put inside the pipes in order to achieve the desired V. The dimensions and weight per foot of the pipe and #3 rebar are provided in Table 4.3.

Table 4.2 Pipe and rebar dimensions and weight

Pipe diameter (in)	4.25
Pipe thickness (in)	0.357
Pipe weight per foot (lb/ft)	2
#3 rebar diameter (in)	0.375
#3 rebar weight per foot (lb/ft)	0.376

Due to the weight of the pipe, limitations of the motor, and the configuration of the load system, the pipe was lowered by hand into the large tank (care was taken in order to lower the pipe as uniformly as possible). For Test 4, a measuring tape was used to measure the depth to the top of the pipe and the depth to the clay surface to determine the amount embedded. For all the other tests, a linear variable differential transformer (LVDT) was placed above the bolt located at the top of the pipe to measure the vertical displacement as a function of time. Since the LVDT could not be installed at the same moment that the pipe was placed, the initial embedment had to be estimated by visual inspection.

4.5 INITIAL EMBEDMENT ESTIMATION

Since the pipe is being lowered relatively fast in both embedment tests, it is assumed that the initial embedment occurs in undrained conditions. The amount of embedment was estimated using the procedure described by Simpson et al. (2015). It should be noted that this method was originally fitted for an embedment up to a embedment diameter ratio (z/D) of 0.5 and may underpredict the penetration resistance and initial embedment for pipes with greater embedment.

4.6 RESULTS

4.6.1 SMALL TANK, 3-FT LONG PIPE

For the 3-ft long pipe embedment tests, the vertical displacement measured with the LMT was plotted versus time to provide a displacement curve (semi-logarithmic). Curves for tests 1 through 3 are provided in Figures 4.3 through 4.5, respectively.

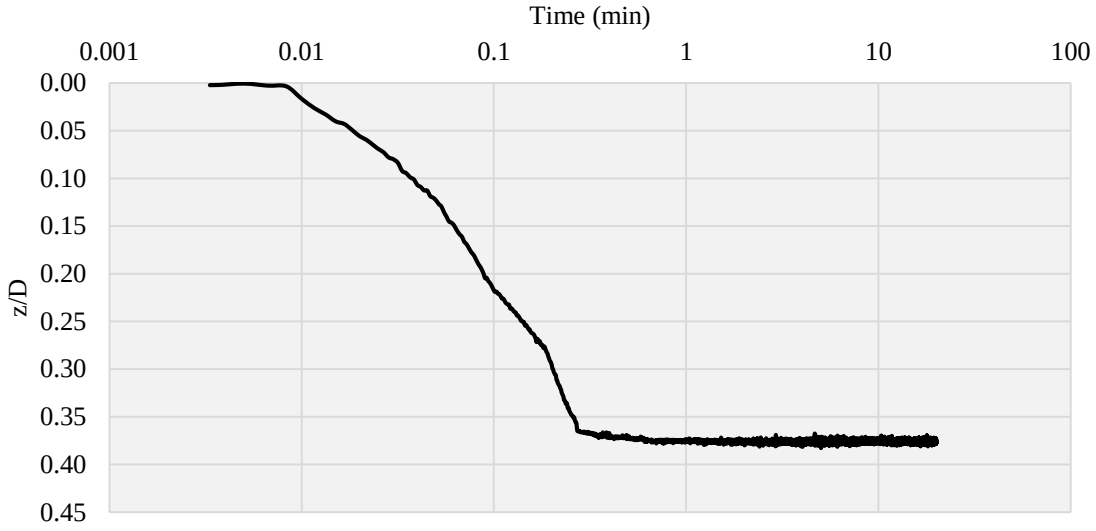

Figure 4.3 Embedment versus log(time) for Test 1

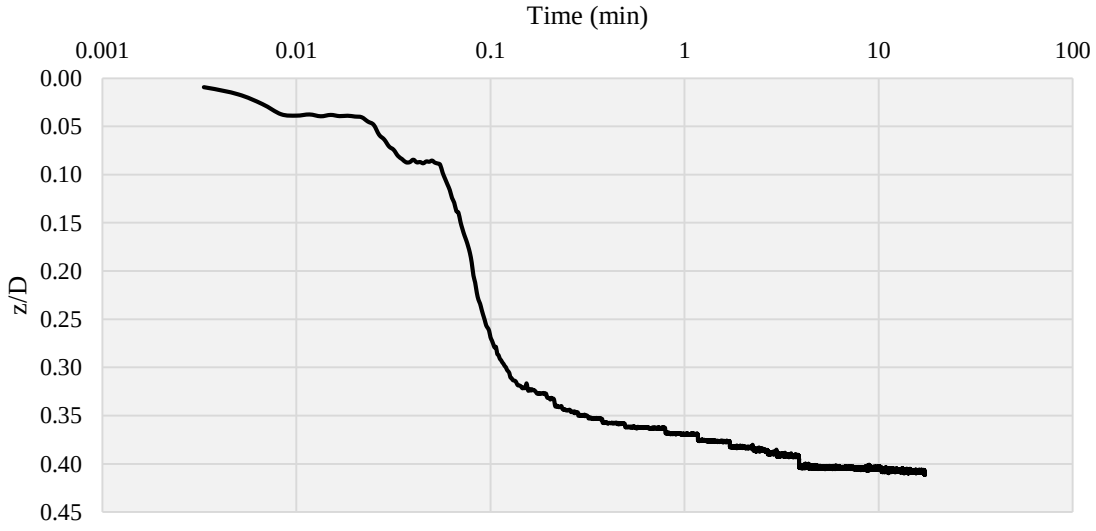

Figure 4.4 Embedment versus log(time) for Test 2

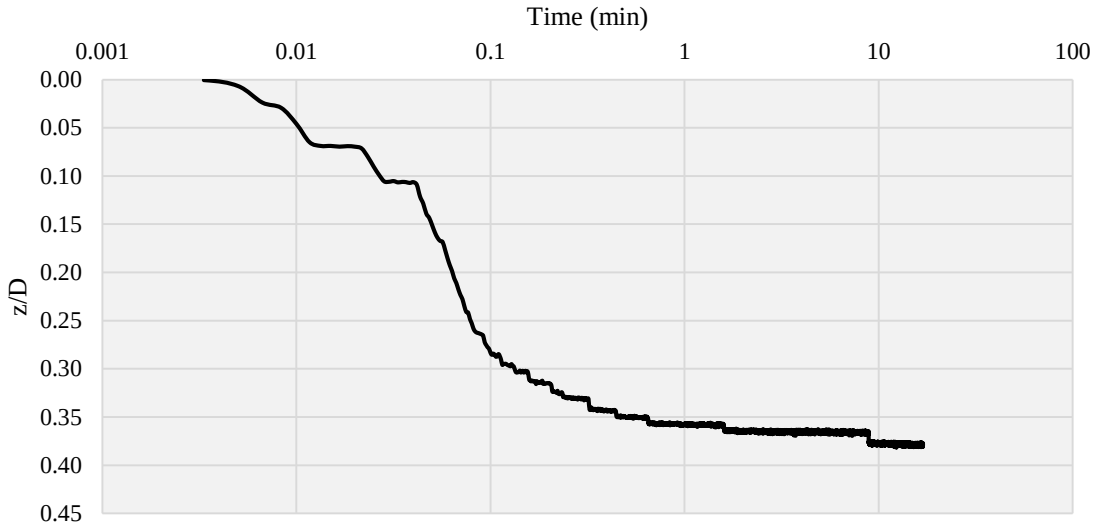

Figure 4.5 Embedment versus log(time) for Test 3

Since the amount of water above the clay surface was not measured, the initial pipe embedment was estimated with a water layer thickness of 1, 1.5, and 2 in. It was found that the thickness of the water layer was not significantly sensitive to +/- 0.5 in of water. The results of this sensitivity analysis are shown in Figure 4.6. The water level above the clay is important because the increase in effective stress acting on the clay due to the weight of the pipe directly depends on the portion of the pipe that is submerged.

A summary of the 3-ft long pipe embedment test results, as well as the estimations using the procedure outlined in Simpson et al. (2015) (assuming 1.5 inches of water on top of the clay), are provided in Table .3. The values of predicted embedment are consistent with the measured embedment, with a relative difference between the two values ranging from -1.9% to 11.0%.

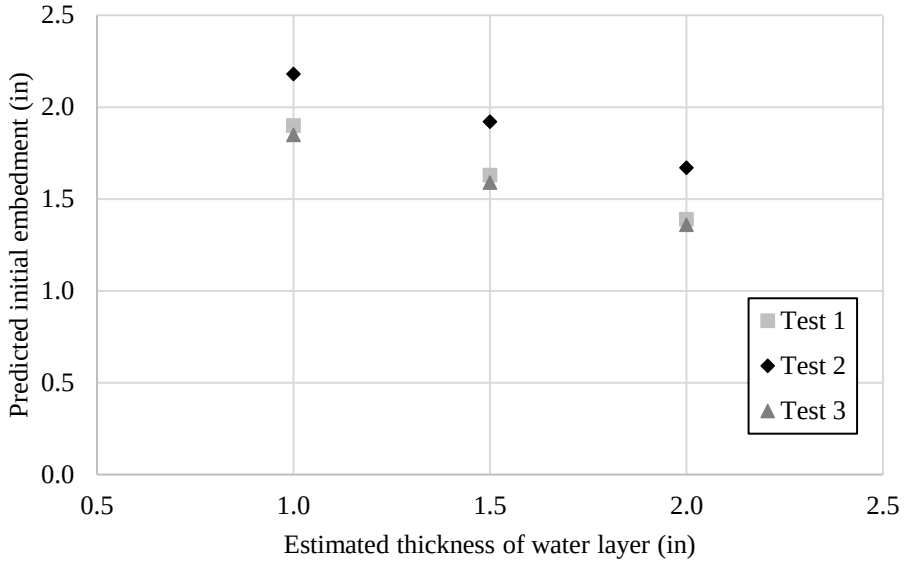

Figure 4.6 Sensitivity analysis results of estimated thickness of water layer, z_w

Table 4.3 3-ft pipe embedment test results

Test No.	**$S_{u,r}$ (psf)**	**w (%)**	**V (lb/ft)**	**$z_{ini}^{Meas.}$ (in)**	**$z_{ini}^{Est.}$ (in)**	**$z_{ini}^{Est.}$ / z_{ini}^{Meas}**
1	1.9	125	4.47	1.61	1.63	1.01
2	1.4	125	4.03	1.73	1.92	1.11
3	2.0	128	4.54	1.62	1.59	0.98

4.6.2 LARGE TANK, 6-FT, 9-FT AND 10-FT LONG PIPES

A summary of the test results, as well as the estimations using the procedure recommended by Simpson et al. (2015) are provided in Table 4.4. In general, the predicted embedment does not significantly differ from the measured embedment (except Test 7). The relative difference between the two values range from -45.0% to 28.9%.

The vertical displacement data recorded by the LVDT for Tests 6, 7, 8 and 9 are presented in Figures 4.7 and 4.8, 4.9 and 4.10, respectively. Based on the settlement curves for Tests 6, 7, 8 and 9, the coefficient of consolidation (c_v) can be estimated using Equation

2.11. For this case, the drainage distance can be considered as the pipe diameter (Krost et al. 2010). However, since the settlement curves are not complete, t_{90} (the time required to achieve a degree of consolidation of 90%) is not known and an assumption must be made. A hypothetical settlement curve is plotted along with the measured settlement curves, with the assumptions that the amount of settlement recorded corresponds to approximately 90% of the total settlement and c_v = 0009 ft^2/day (0.3 m^2/year). The hypothetical and the measured settlement curves agree well for all the tests. This value of c_v is also in agreement with values reported in the literature for Gulf of Mexico clay (Taukoor and Rutherford, 2016; FUGRO, 2005).

If the pipe is modelled as a strip footing, 1D consolidation is assumed, the coefficient of compression (C_C) can be estimated using Equation 4.1. When calculating σ'_1 and σ'_2, the thickness of the clay layer was assumed to be 1.5D and the stresses were calculated at the middle of the layer. The initial penetration of the pipe was accounted for when calculating σ'_2 by assuming the stress is applied at the pipe invert and not at the soil surface. The final settlement used in the calculations was obtained from the hypothetical settlement curve used to estimate c_v. The results are summarized in Table 4.5. The values range from 0.71 to 1.26, with an average value of 0.78.

$$C_c = C_{C\varepsilon}(1 + e_0) \quad \text{(Eq. 4.1)}$$

$$C_{C\varepsilon} = \frac{\Delta\varepsilon}{\log(\frac{\sigma'_2}{\sigma'_1})} \quad \text{(Eq. 4.2)}$$

$$e_0 = \frac{wG_s}{S} \quad \text{(Eq. 4.3)}$$

Where:

C_C = Coefficient of compression;

$C_{C\varepsilon}$ = Modified compression index or compression ratio;

σ'_1 = Initial effective normal stress (before placing the pipe);

σ'_2 = Final effective normal stress (after placing the pipe);

e_0 = Initial void ratio;

w = water content;

G_s = specific gravity (G_s = 2.75);

S = degree of saturation (S = 1).

Table 4.4 Summary of test results

Test No.	**$S_{u,R}$ (psf)**	**w (%)**	**V (lb/ft)**	**$z_{ini}^{Meas.}$ (in)**	**$z_{ini}^{Est.}$ (in)**	**$z_{ini}^{Est.}$ / z_{ini}^{Meas}**
4	1.5	142	6.01	2.9	3.6	1.24
5	1.3	140	4.05	1.9	2.2	1.16
6	1.4	138	2.8	1.3	1.1	0.85
7	1.4	138	2.8	2.0	1.1	0.55
8	2.5	107	6.0	1.4	1.8	1.29
9	2.5	107	6.0	2.3	1.8	0.78

Table 4.5 Estimated coefficient of compressibility (C_c)

Test No.	Coefficient of compressibility (Cc)
6	0.73
7	1.26
8	0.41
9	0.71

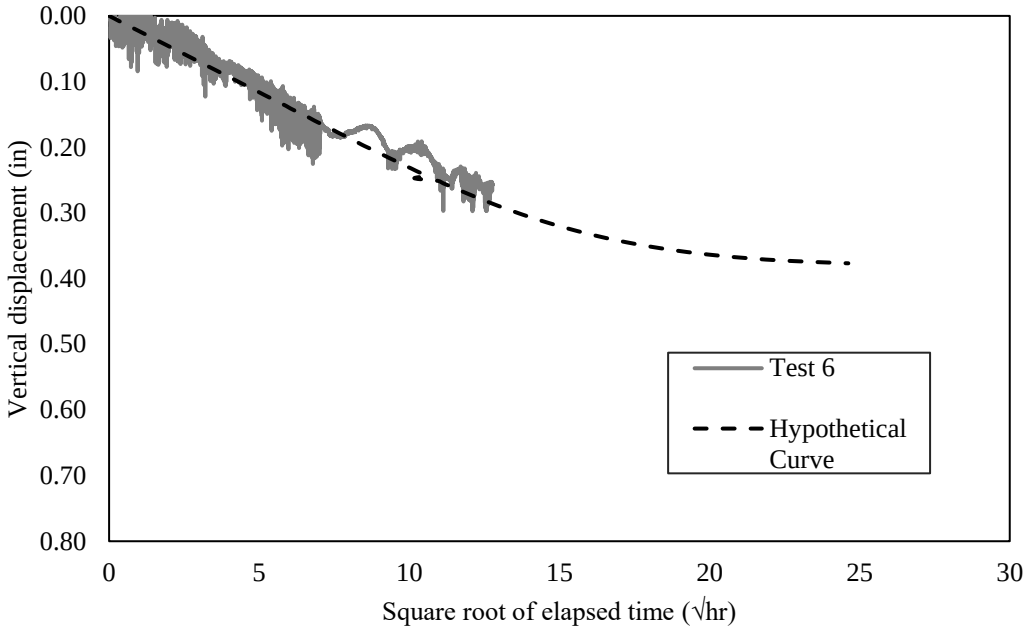

Figure 4.7 Settlement curve (Test 6)

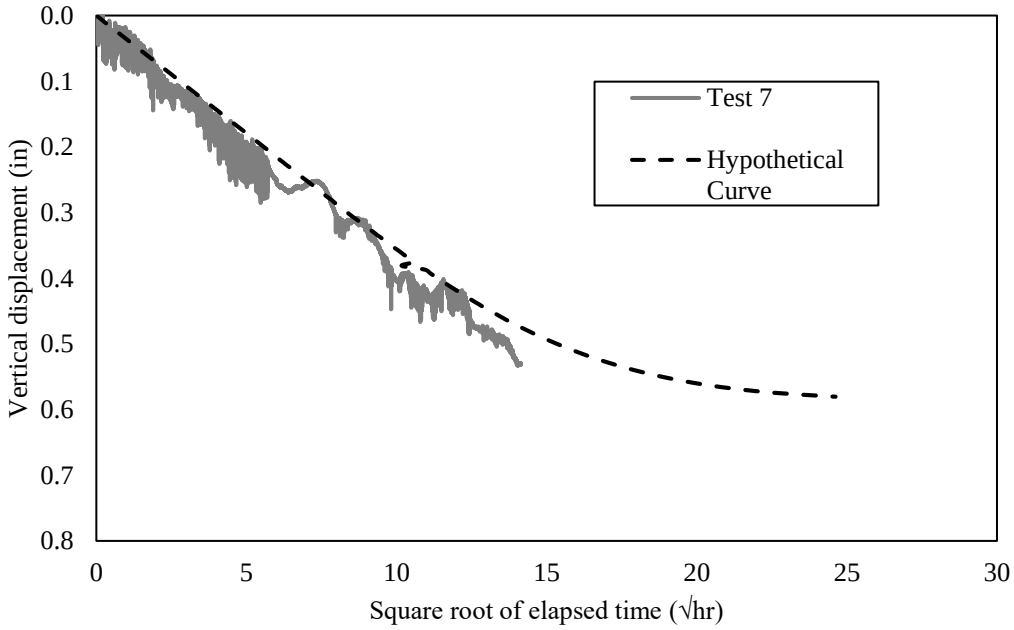

Figure 4.8 Settlement curve (Test 7)

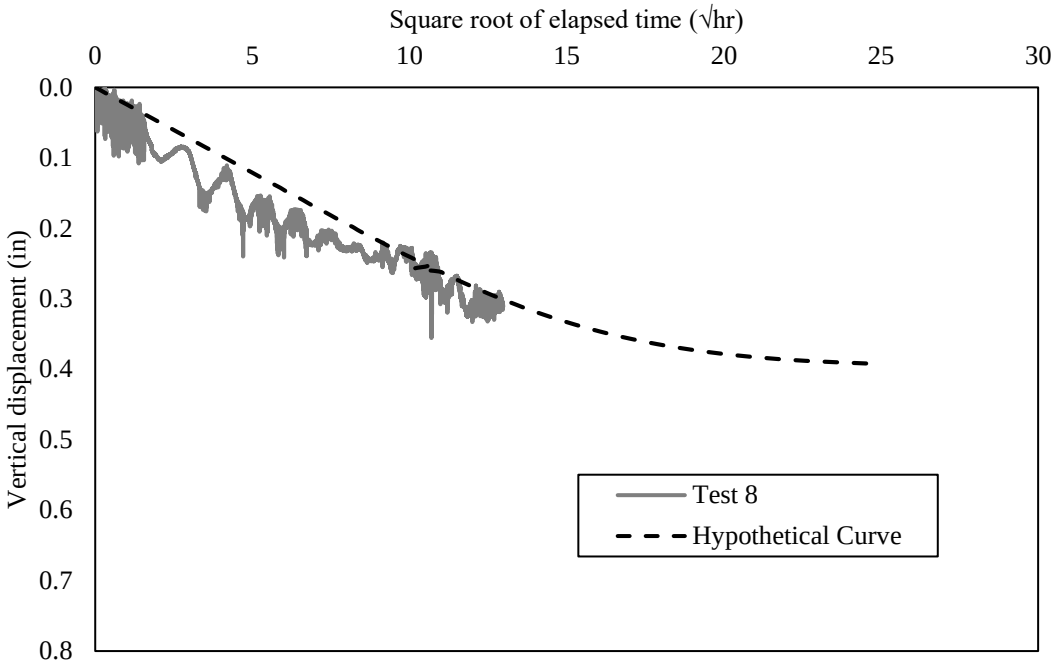

Figure 4.9 Settlement curve (Test 8)

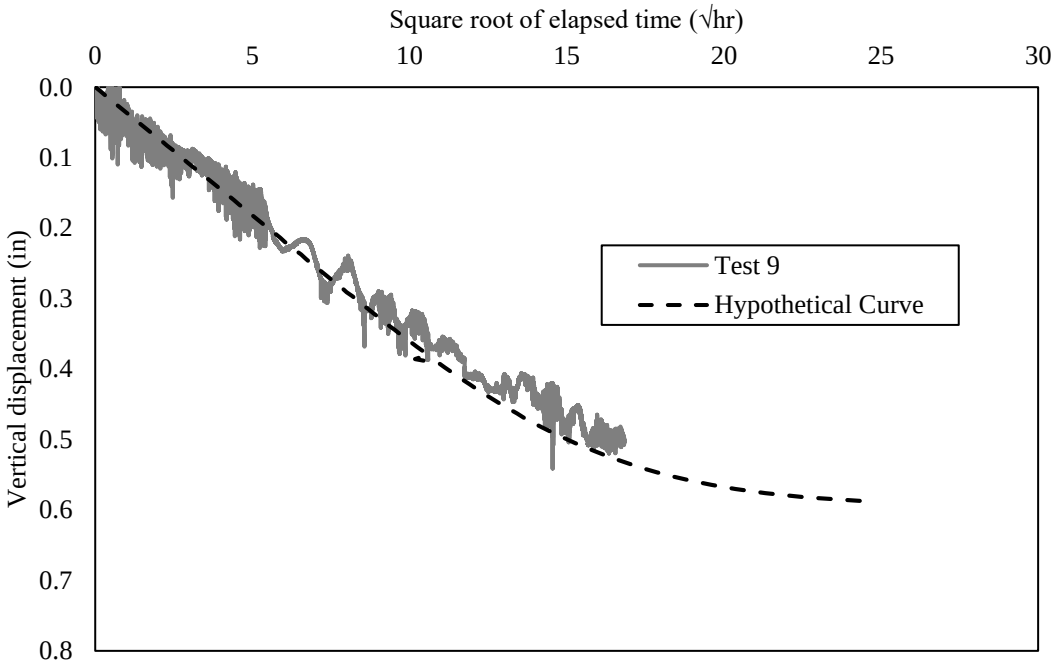

Figure 4.10 Settlement curve (Test 9)

4.7 CONCLUSIONS

In this study, embedment tests of 3-ft, 6-ft, 9-ft and 10-ft long sections of a polypropylene pipe in Gulf of Mexico clay were performed to compare the predicted of initial pipe embedment using the equation outlined in Simpson et al. (2015) to the initial embedment obtained from laboratory tests. Additionally, the coefficient of consolidation and the coefficient of compression for the Gulf of Mexico clay are estimated based on the settlement measurements following laying of the pipe. The following conclusions can be drawn:

1. The method outlined in Simpson et al. (2015) for estimating initial embedment performed well for the 3-ft long pipe.
2. The method outlined in Simpson et al. (2015) provides a starting point for larger-scale tests (i.e. 10-ft long pipe) where V can be controlled.
3. The initial embedment is a bearing capacity failure and the method presented by Simpson et al. (2015) only provides an estimate of the initial vertical displacement. The estimation for initial embedment does not account for settlement of the clay. Thus, in order to determine the required V to achieve a certain amount of embedment, the settlement of the clay must be calculated.
4. A hypothetical consolidation curve assuming c_v = 0.009 ft^2/day (0.3 m^2/year) and a final settlement 10% greater (U = 90%) than the values recorded approximately two weeks after the clay was mixed is in good agreement with the measured settlement, indicating that a significant part of the consolidation seems to occur approximately two weeks after the pipe is laid on the soil bed.
5. The coefficient of compression (C_c) of the Gulf of Mexico clay was estimated by modeling the pipe as a strip footing and assuming 1-D consolidation. The results range from 0.71 to 1.26, with an average value of 0.78. This broad range may be attributed to the

assumptions used in the model and due to the uncertainties associated with hand-placing the pipes. These uncertainties are linked to measuring different initial embedment for pipes with similar unit weight and the time at which the settlement starts being recorded, which can take several minutes. Due to this time delay to start measuring the settlement after laying, capturing the moment where the “initial embedment” ceases and the settlement is dictated by consolidation may be cumbersome.

Chapter 5: Tilt Table Tests

5.1 Introduction and Objectives

The objective of this chapter is to obtain the drained residual shear strength of interfaces between flowlines and surrounding soils at low effective normal stresses by performing tilt table tests. Gulf of Mexico clays and a polypropylene solid interface are used to represent the soil in the seabed and flowlines coating, respectively.

5.2 Test Materials

5.2.1 Soil

Marine clay samples obtained from three different locations in the Gulf of Mexico was used in the testing and in this study will be referred to as S1, S2 and S3. After being extracted from the Shelby tubes (Figure 5.1), the samples were stored in Ziploc containers and bags (Figure 5.2).

Figure 5.1 Shelby tubes

Figure 5.2 Ziploc container and bag

5.2.2 SOLID INTERFACE

A natural polypropylene solid interface (Interface 1) of dimensions 14 x 8 x 0.25 in was used in this study (Figure 5.). The solid interface material is typical commercially available and was obtained from a local plastic supplier store. The interface is attached to a flat steel plate with 14 x 8in in area and about 1 in thick. Another interface (Interface 2) specified as the same material as the one shown in Figure 5.3 but obtained from a different manufacturer is shown in Figure 5.4.

Figure 5.3 Polypropylene solid interface (Interface 1)

Figure 5.4. Additional polypropylene solid interface (Interface 2)

5.2.3 SALT WATER

The salt water used in the testing was prepared by mixing commercial-grade sea salt with tap water. A target salinity of approximately 35 parts per thousand (35g/L) was used in order to simulate salt water in the Gulf of Mexico sea. The salinity of the water was measured using a hydrometer (Figure 5.5).

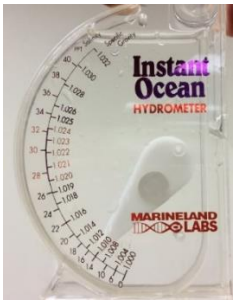

Figure 5.5. Hydrometer for salinity measurement

5.3 TEST APPARATUS

5.3.1 TESTE DEVICE

The tilt table device is composed by an aluminum base plate that is 24 x 24 in (700 x 700 mm) in area and is hinged to a steel frame (Figure 5.6). The solid interface is attached to the base plate with clamps. In order to generate shear stress, a winch is used to lift the free end of the base plate up to the desired inclination. The maximum tilting angle of the device is approximately 45º.

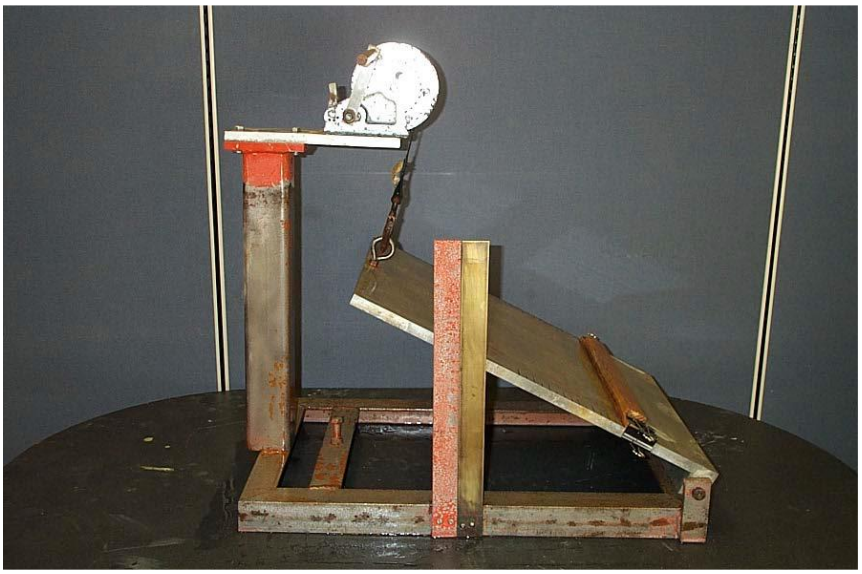

Figure 5.6. Tilt table device.

5.3.2 LOADING PLATES

The load is applied to the specimen (soil + interface) by a loading plate placed on top of the soil specimen. In this study, an acrylic plate was used and referred to as LP. The plate has a thickness of about 1 in (25.4mm) and an area of 6 x 6 in (152 x 152 mm). A non-woven geotextile is attached to the bottom of the loading plate in order to allow free drainage at the top of the specimen. This type of geotextile was chosen as the drainage material because it is rough enough so that failure does not occur between the loading plate and the soil specimen and smooth enough so that it does not protrude into the soil specimen. Table 5.1 contains the information about the weight of the loading plate. The loading plate with the geotextile is shown in Figure 5.7.

Figure 5.7 Acrylic loading plate with geotextile

Table 5.1 Loading Plate Weight

Loading Plate	Weight in Air (lb)	Submerged Weight (lb)
LP	1.58	0.22

5.3.3 LOADING WEIGHTS

Steel weights were used to apply to surcharge stress on the specimen (Figure 5.8). The relevant information about the weights used in this study are summarized in Table 5.2.

Figure 5.8 Steel Weights

Table 5.2 Information about loading weights

Identification	Thickness		Weight in Air		Submerged Weight		Effective Normal Stress on Horizontal Plane	
	cm	in	kg	lb	kg	lb	kPa	psf
W1	1.94	0.76	2.52	5.55	1.57	3.45	0.64	13.35
W2	0.69	0.27	1.25	2.75	0.77	1.69	0.31	6.53
W3	2.67	1.05	3.65	8.04	2.43	5.35	0.99	20.70
W5	2.50	0.98	3.65	8.04	3.14	6.91	1.28	26.73
W9	2.50	0.98	10.00	22.03	8.57	18.88	3.50	73.02

5.4 TEST PROCEDURE

The test method basically consists of applying a static load to a clay resting on a horizontally oriented interface, allow the clay to fully consolidate under the applied normal stress, and then tilt the interface in order to apply shear stress at a slow rate to achieve drained conditions until failure occurs. A schematic of the test method is shown in Figure 5.9.

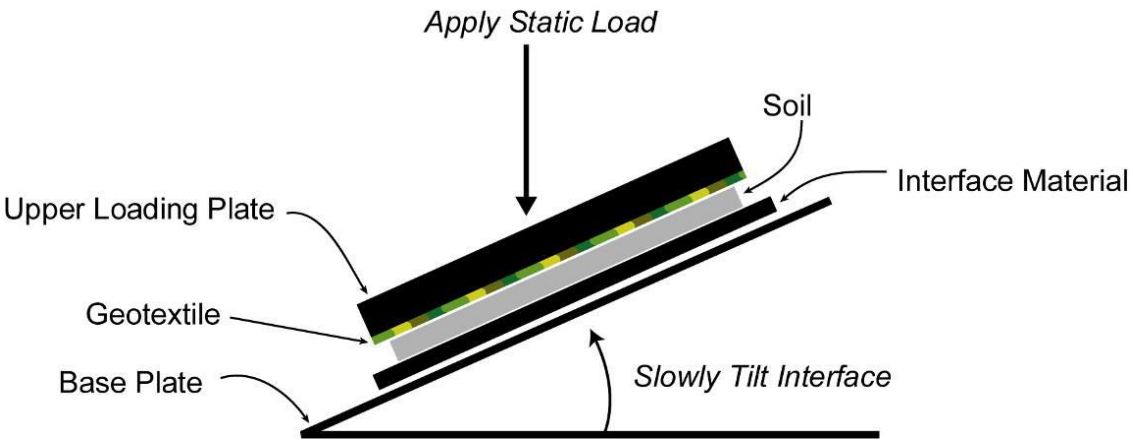

Figure 5.9 Schematic of tilt table test method (Bae, 2009).

Najjar et al. (2003) and Najjar et al. (2007) explain in detail the test procedures. A few modifications were made in the test procedure in order to add some conservatism and ensure fully drained conditions during testing for the clays used in this study. The test procedures used in this study are as follows:

- *Specimen Preparation:*

Since the drained strength is of interest, the initial soil structure is not relevant, thus, the clay is placed in the remolded state, being close to the fully softened state, which minimizes the displacements to achieve drained conditions.

The specimens were prepared in a bucket to a desired water content by adding tap water and mixing thoroughly until homogeneity was achieved. The desired water content is obtained by linearly extrapolating the virgin compression curve from 1D consolidation test data back to the desired normal stress values. For typical marine clays, this value should exceed the liquid limit of the clay (Najjar et al. 2003). The target water content (typically near or above the liquid limit) had to be sufficiently high to assume a value greater than the water content in which the soil specimen would be in equilibrium (after consolidation)

for an applied normal stress, but also sufficiently low so that specimen preparation would be feasible. The clay was transferred from the bucket to Ziploc bags or Tupperware containers (stored inside Ziploc bags).

The clay is uniformly spread on the polypropylene interface with the help of a wood mold and a spatula in order to cover an area close to 6.5 x 6.5 in (165 x 165 mm) and have 0.08 in (2 mm) in thickness (Figure 5.10). This thickness was chosen because it had to be small enough so that consolidation and shearing times are minimized, but also had to be large enough so that bearing capacity failure would not occur when applying the normal stress and the geotextile would not protrude into the soil specimen.

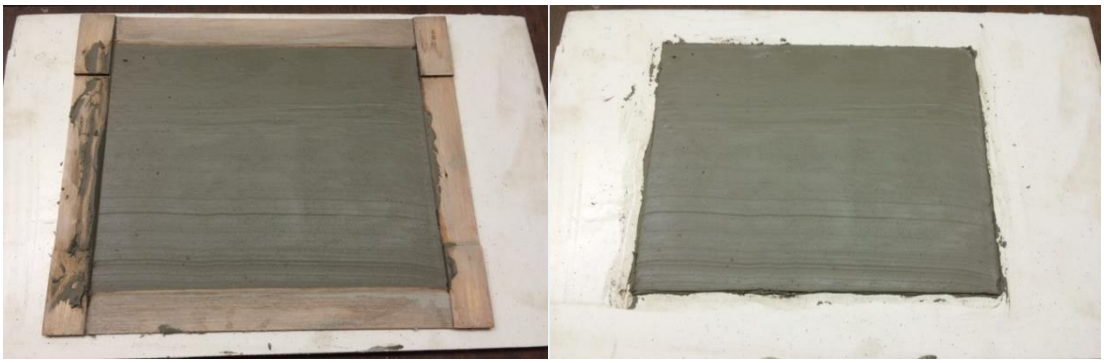

Figure 5.10 Specimen Preparation with wood mold.

- *Consolidation:*

After spreading the clay uniformly on the polypropylene interface, the loading plate is placed on the top of the soil specimen and half of the desired normal stress is applied. The specimen is left to consolidate until a degree of consolidation (U) of at least 95% is achieved. After that, the specimen is inserted into a bath of water in a 47 in-diameter (1,200 mm) aluminum tank with a height of 23.6 in (600 mm). The remaining of the desired

normal stress is then applied and the soil specimen is once again left to consolidate until a degree of consolidation of at least 95% (U_{95}) is achieved (Figure 5.11).

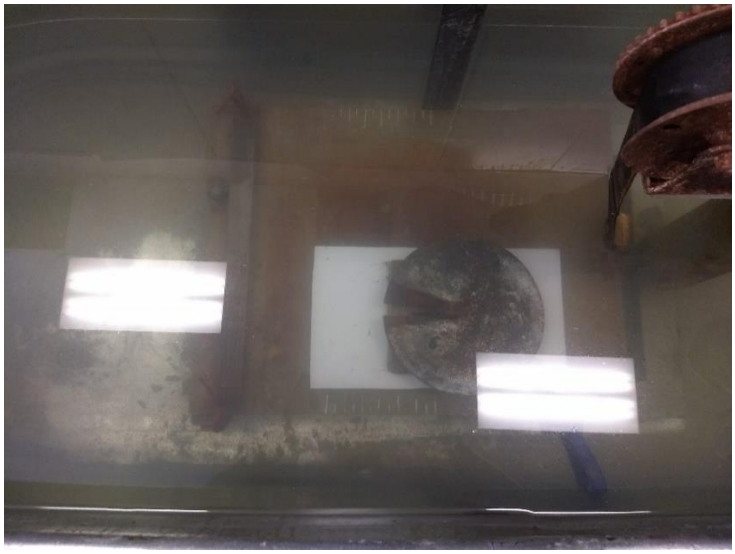

Figure 5.11 Consolidation stage

For the case of a single drainage boundary (it is assumed that water can only drain at the boundary where the geotextile is located), the average time to achieve U_{95} can be estimated by assuming 1D consolidation using the following equation:

$$t_{95} = \frac{T_{95}H^2}{c_v} \quad \text{(Eq. 5.1)}$$

Where T_{95} = time factor; c_v = coefficient of consolidation and H = drainage distance (specimen thickness). For this case, T_{95} = 1.129 and H = 2mm. Najjar et al. (2003) points out that for low normal stresses there is a strong possibility that drainage also occurs along the interface, thus, assuming a single drainage boundary introduces some conservatism when calculating t_{95}. The coefficient of consolidation can be obtained from a 1D consolidation test performed at the desired normal stress using soil at the remolded states,

c_v = 0.3m^2/yr was used instead, based on the tests embedment tests described in Chapter 4 and on values reported in the literature (Gerkus, 2016; Lai, 2017; FUGRO, 2005)

Based on Equation 5.1, a time interval of approximately 8 minutes or greater will achieve equilibrium under the applied normal stress. In order to consider the uncertainties in the coefficient of consolidation used in the calculations, the soil specimen is left to consolidate for approximately 15 minutes per load increment during the consolidation stage.

- *Shearing:*

After consolidation of the clay, the process of shearing starts by lifting the base plate from the horizontal (Figure 5.12). Since drained conditions must be achieved in this process, the table must be lifted slow enough to allow dissipations of excess pore pressure generated during the shearing process. Gibson and Henkel (1954) suggests that the time to failure (t_f) to achieve drained conditions in a direct shear test is given by the following equation:

$$t_f = 50t_{50} \quad \text{(Eq. 5.2)}$$

Where t_{50} is the time required to a degree of consolidation of 50% assuming 1D consolidation. t_{50} can be calculated using Equation 5.1 considering T_{50} = 0.197. The time to failure obtained using Equation 5.2 is only valid given that the rate of deformation is constant throughout the test. Since the tilt-table test resembles a load-controlled type of test, the deformations in the soil and at the interface are expected to assume larger values as shear progress. As an attempt to try to maintain the deformation constant throughout the test, larger load increments are applied to the specimen at early stages of the test, where

shear deformations are expected to be small. When the specimen approaches failure, smaller load increments are applied due to expected large shear deformations at this stage.

Figure 5.12 Shearing Stage

The process of lifting the base plate to achieve the drained residual strength of the soil specimen can be described as follows. For the first four increments the tilt table is increased in 5-degree steps and the soil specimen is left to drain for a period of 5 minutes per increment. After that, the load step is cut down to 2 degrees per increment for another five increments and the soil specimen is left do drain for 5 minutes per increment. After reaching an angle of 30 degrees, the load step is cut down to 1 degree per increment and the soil is left to drain for 10 minutes until failure occurs. Failure occurs when the sample slides approximately 0.5 in or (12.7 mm). Since for some tests the sliding movement was not slow enough and the amount of slip could not be easily controlled, a movable wooden rod (Figure 5.13) was clamped 0.5 in ahead of the sample to prevent further displacement. After that, the base plate is lowered 10 degrees and the sample is left to consolidate for 15 minutes. The wooden rod is shifted down by 0.5 in and the whole process is repeated. In a

typical test, the residual drained strength was reached at a total shear displacement of 1 to 2 in. The tests were conducted until at least three consecutive failures occurred at the same angle.

For samples which failure occurs before reaching 30 degrees, the consolidation time per increment from 20 degrees up was 10 minutes instead of 5 minutes, which is due to the fact that a large amount of excess pore pressure is built up when the soil specimen approaches failure, thus the sample should be left to consolidate for a longer time. Additionally, for these samples, the load step was cut down to 1 degree per increment approximately 4 degrees before the expected angle at which the sample was expected to fail. This was done in order to increase the resolution as the sample approached failure.

The normal force acting on the sample at failure is the weight component that is perpendicular to the plane of the base plate, whereas the shear force is the weight component that is parallel to the plane of the base plate. The effective normal stress and the shear stress are calculated by using the following equations:

$$\sigma' = \frac{W'}{A} cos\beta \quad \text{(Eq. 5.3)}$$

$$\tau = \frac{W'}{A} sin\beta \quad \text{(Eq. 5.4)}$$

Where W' is the submerged weight acting on the sample; A is the cross-sectional area of the loading plate; and β is the angle of inclination of the base plate at failure.

One possible limitation of the tilt-table test is that the applied load is not uniform along the interface due to the overturning moment induced by the eccentricity about the center of gravity of the loading plate as the base plate is tilted. This eccentricity increases as the inclination of the base plate and the applied load increase. In order to minimize the effects caused by this eccentricity, the steel weights used to apply the normal stress on the

sample were chosen carefully with the goal of minimizing the height (combination of the weights thicknesses) above the loading plate, thus minimizing overturning moment. Additionally, the center of gravity of the applied load is moved back in order to balance the overturning moment generated as the angle of inclination increases, which causes the net eccentricity to assume a value close to zero. This is achieved by shifting back the rod attached at the top of the loading plate (Figure 5.7). The amount of which the rod should be shifted back was obtained by trial and error. In order to ensure that the eccentricity was not significant, the interface was inspected visually for signs of eccentric loading, checking if the pitch of the loading plate remained parallel to the base plate and if the failure surface (after removal of the weights and the loading plate) was continuous at the interface between the clay and the polypropylene base.

Figure 5.13 Wooden stopper

5.5 TEST PROGRAM

A total of 50 tilt-table tests were performed using Gulf of Mexico marine clay obtained from three different sources to obtain the drained residual shear strength at the interface of the soil and a polypropylene solid interface (Interface 1). Different normal stresses were applied on the specimens with the purpose of simulating possible loading conditions that the soil could be subjected to in the field. The test program is summarized in Table 5.3. Details of the test program including initial and final water content are presented in Appendix B.

Table 5.3 Summary of Test Program.

Test Number	Soil Source	Effective Normal Stress on Horizontal Plane (psf)
1	S1	7.9
2	S1	7.9
3	S1	7.9
4	S1	14.8
5	S1	14.8
6	S1	14.8
7	S1	16.9
8	S1	16.9
9	S1	16.9
10	S1	22.1
11	S1	22.1
12	S1	22.1
13	S1	40.6
14	S1	40.6
15	S1	40.6
16	S1	93.8
17	S1	93.8
18	S1	114.2
19	S1	114.2
20	S1	114.2
21	S2	7.4
22	S2	7.4
23	S2	7.4
24	S2	16.9
25	S2	16.9
26	S2	16.9
27	S2	39.8
28	S2	39.8
29	S2	39.8
30	S2	93.8
31	S2	93.8
32	S2	93.8
33	S2	146.9
34	S2	146.9
35	S2	146.9
36	S3	7.4
37	S3	7.4
38	S3	7.4
39	S3	16.9
40	S3	16.9
41	S3	16.9
42	S3	39.8
43	S3	39.8
44	S3	39.8
45	S3	93.8
46	S3	93.8
47	S3	93.8
48	S3	146.9
49	S3	146.9
50	S3	146.9

5.6 TEST RESULTS AND DISCUSSION

A summary of the tests results is presented in Table 5.4. The results include the measured values of drained residual secant friction angles and friction coefficients for the soil obtained from three different sources when tested with polypropylene solid interface (Interface 1). The secant friction angle is defined as the arc tangent of the ratio of the shear stress to the effective normal stress at failure. The friction coefficient is defined as the ratio of the shear stress to the effective normal stress at failure.

- *Failure Mechanism:*

Figure 5.14 shows an illustration of the failure mechanism observed in all drained interface tests. It shows that the failure mechanism is characterized by complete sliding of the clay over the solid interface. This mechanism can be identified by observing the 1.5 in long section of clear interface right behind the loading plate, indicating that the clay completely slid over the interface.

The clear interface behind the loading plate after failure also indicates that the shear rate used in the tests was slow enough to achieve drained conditions, because if a higher rate had been used the failure mechanism would have occurred internally to the clay layer rather than at the interface. This can be explained by the fact that the shear induced excess pore pressures will be greatest near the middle of the clay layer possibly leading to a premature failure there under undrained conditions, or at least, not fully-drained conditions (Najjar et al., 2003). A few tests were conducted at a significantly faster rate and it was noted that the failure mechanism occurred internally to the clay, supporting the believe that, for those tests, drained conditions were not achieved (due to limited data, the results of these tests are not included in this document).

The observation of the failure mechanism also allowed to investigate the possibility of the geotextile protruding into the clay, thus contacting the interface and affecting the interface strength. Observation of the specimens during and after failure indicated no signs of noticeable protrusion of the geotextile into the clay. Additionally, these observations showed that the upper loading plate remained parallel to the base plate and no noticeably pitch due to eccentricity occurred, which indicates that the eccentricity during the tests was not significant and therefore did not affect the results. Moreover, the eccentricity after failure was calculated for all normal stresses applied on the specimens and the values obtained were all significantly smaller than one quarter of the length of the loading plate.

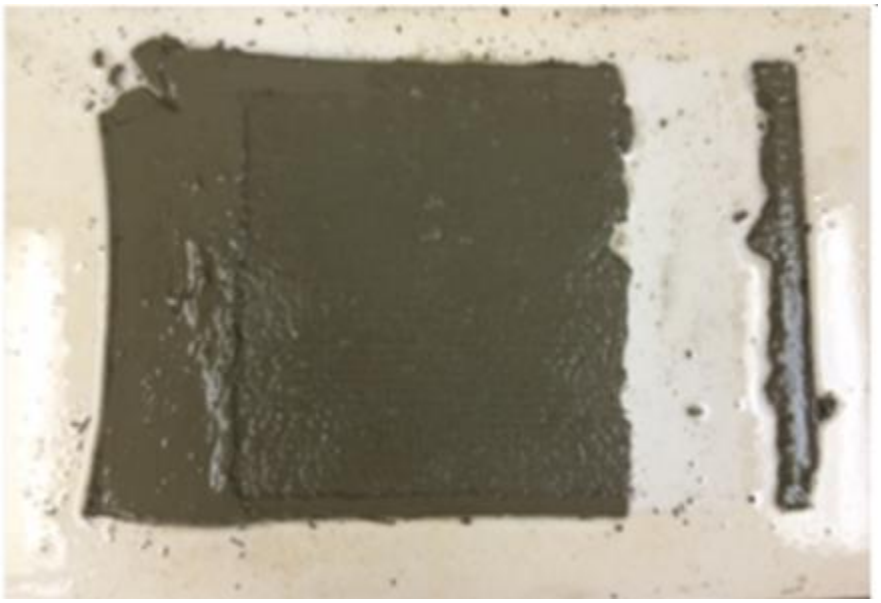

Figure 5.14 Interface failure

Table 5.4 Summary of Test Results.

Test Number	Soil Source	Effective Normal Stress on Horizontal Plane (psf)	Drained Residual Secant Friction Angle (deg)	Coefficient of Friction	Effective Normal Stress at Failure (psf)	Residual Shear Strength (psf)
1	S1	7.9	36.0	0.73	6.4	4.6
2	S1	7.9	36.0	0.73	6.4	4.6
3	S1	7.9	36.0	0.73	6.4	4.6
4	S1	14.8	33.0	0.65	12.4	8.1
5	S1	14.8	33.0	0.65	12.4	8.1
6	S1	14.8	33.0	0.65	12.4	8.1
7	S1	16.9	31.0	0.60	14.5	8.7
8	S1	16.9	30.5	0.59	14.6	8.6
9	S1	16.9	30.5	0.59	14.6	8.6
10	S1	22.1	30.0	0.58	19.1	11.1
11	S1	22.1	29.5	0.57	19.2	10.9
12	S1	22.1	30.0	0.58	19.1	11.1
13	S1	40.6	28.0	0.53	35.8	19.1
14	S1	40.6	28.0	0.53	35.8	19.1
15	S1	40.6	27.5	0.52	36.0	18.7
16	S1	93.8	24.5	0.46	85.4	38.9
17	S1	93.8	26.0	0.49	84.3	41.1
18	S1	114.2	24.0	0.45	104.3	46.4
19	S1	114.2	24.0	0.45	104.3	46.4
20	S1	114.2	24.0	0.45	104.3	46.4
21	S2	7.4	37.0	0.75	5.9	4.5
22	S2	7.4	36.0	0.73	6.0	4.3
23	S2	7.4	36.0	0.73	6.0	4.3
24	S2	16.9	32.5	0.64	14.3	9.1
25	S2	16.9	33.0	0.65	14.2	9.2
26	S2	16.9	34.0	0.67	14.0	9.5
27	S2	39.8	30.0	0.58	34.5	19.9
28	S2	39.8	30.0	0.58	34.5	19.9
29	S2	39.8	30.0	0.58	34.5	19.9
30	S2	93.8	26.0	0.49	84.3	41.1
31	S2	93.8	25.0	0.47	85.0	39.6
32	S2	93.8	26.0	0.49	84.3	41.1
33	S2	146.9	23.0	0.42	135.2	57.4
34	S2	146.9	23.0	0.42	135.2	57.4
35	S2	146.9	23.0	0.42	135.2	57.4
36	S3	7.4	37.0	0.75	5.9	4.5
37	S3	7.4	36.5	0.74	5.9	4.4
38	S3	7.4	37.0	0.75	5.9	4.5
39	S3	16.9	36.0	0.73	13.7	9.9
40	S3	16.9	35.0	0.70	13.8	9.7
41	S3	16.9	35.0	0.70	13.8	9.7
42	S3	39.8	31.00	0.60	34.1	20.5
43	S3	39.8	32.00	0.62	33.8	21.1
44	S3	39.8	32.00	0.62	33.8	21.1
45	S3	93.8	29.0	0.55	82.0	45.5
46	S3	93.8	29.0	0.55	82.0	45.5
47	S3	93.8	29.5	0.57	81.6	46.2
48	S3	146.9	28.0	0.53	129.7	69.0
49	S3	146.9	29.0	0.55	128.5	71.2
50	S3	146.9	28.0	0.53	129.7	69.0

- *Nonlinearity of Drained Residual Strength Envelope*

The results presented in Table 5.4 are plotted in Figures 5.15, 5.16 and 5.17, showing the variation of the residual shear strength, the residual secant friction angle, and the coefficient of friction versus effective normal stress at failure, respectively. Since the effective normal stress decreases as the tilting angle increases (Equation 5.3), the effective normal stresses at failure are not equal to the nominal values presented in Table 5.3.

The interface residual secant friction angle decreases as the effective normal stress increases, which agrees with tilt-table interface tests results conducted on similar soil and similar interface (polypropylene) by Najjar et al. (2007), as shown in Figure 5.18. By comparing the results obtained using each soil, it can be inferred that, for the entire range of stress levels used in this study, soil S3 shows the highest values of interface residual shear strength, while soil S2 shows values greater than the ones obtained using soil S1 (Figure 5.19). Additionally, including the test results obtained by Najjar et al. (2003) and Najjar et al. (2007) using similar soil and similar interface, the average coefficient of friction is about +/-13% at an effective normal stress of approximately 90psf (86.0-93.8psf).

A general relationship between coefficient of friction and effective normal stress for all the soils used in this study can be estimated by using linear regression with the data shown in Figure 5.17. The effective normal stress is normalized by the atmospheric pressure (2116.2 psf). This relationship is expressed in a semi-log plot shown in Figure 5.20.

- *Creep Tests*

In order to check if drained conditions were indeed achieved in the tilt-table tests, creep tests were performed for each soil at the same effective normal stress. The test was conducted as follows. After reaching three consecutive failures at the same angle (at this point a regular test would have been terminated), the test procedure is continued as if one more failure is to be obtained. However, instead of lifting the base plate until another failure occurs, the test is ceased when the angle of inclination is approximately 1 to 2 degrees lower than the expected angle of failure. After approximately 18 hours, the base plate is once again lifted until failure occurs. In all creep tests performed, the angle of inclination at which the specimen failed was the same as the one obtained before the elapsed time interval, which is another indicator that the values of interface residual drained friction angle correspond to drained conditions. The results of the creep tests are summarized in Table 5.5.

Table 5.5 Results of creep tests.

Soil Source	Effective Normal Stress on Horizontal Plane (psf)	Drained Residual Secant Friction Angle (deg)	Time interval (hours)
S1	93.8	24.5	18
S2	93.8	26.0	19
S3	93.8	29.0	18

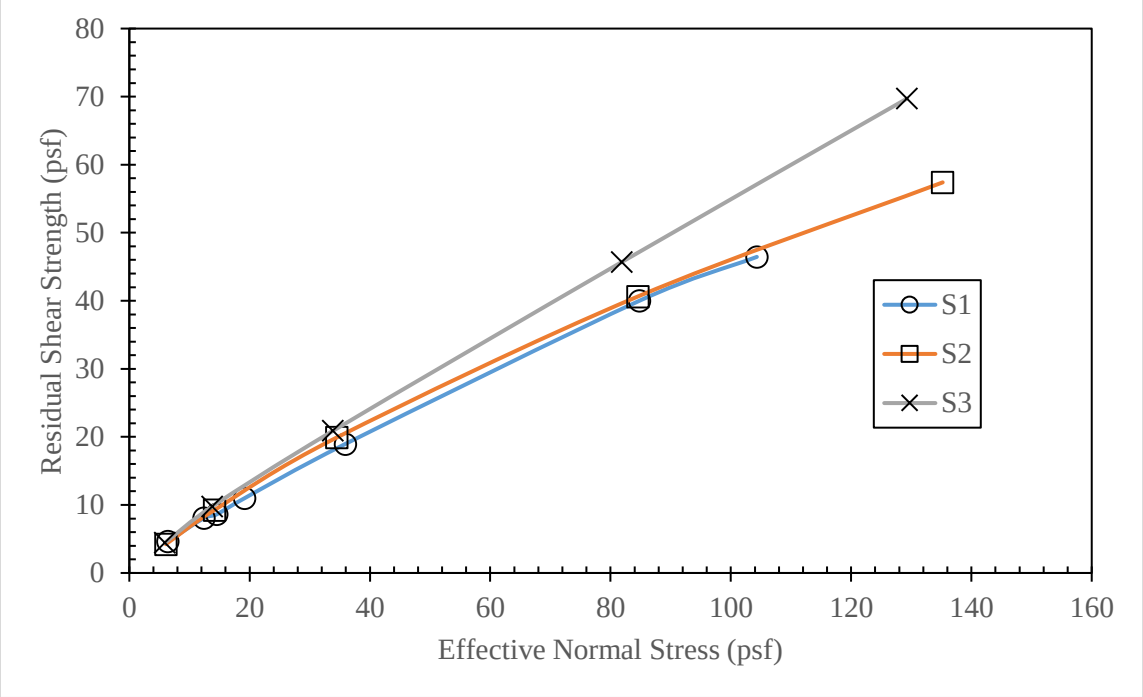

Figure 5.15 Residual shear strength versus effective normal stress.

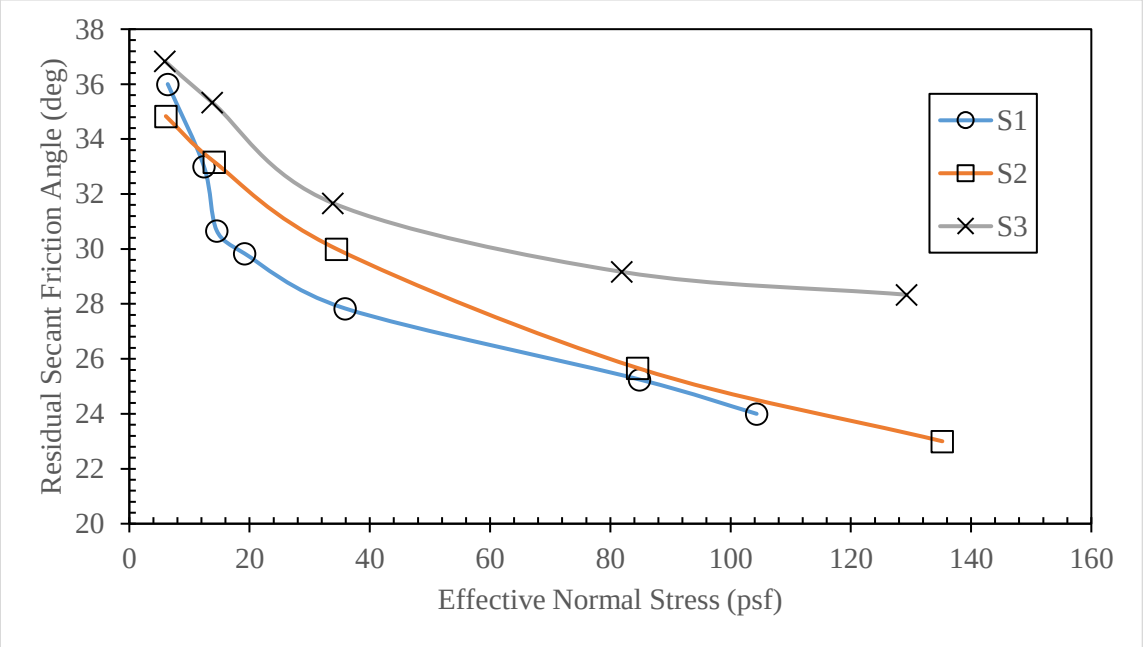

Figure 5.16 Residual secant friction angle versus effective normal stress.

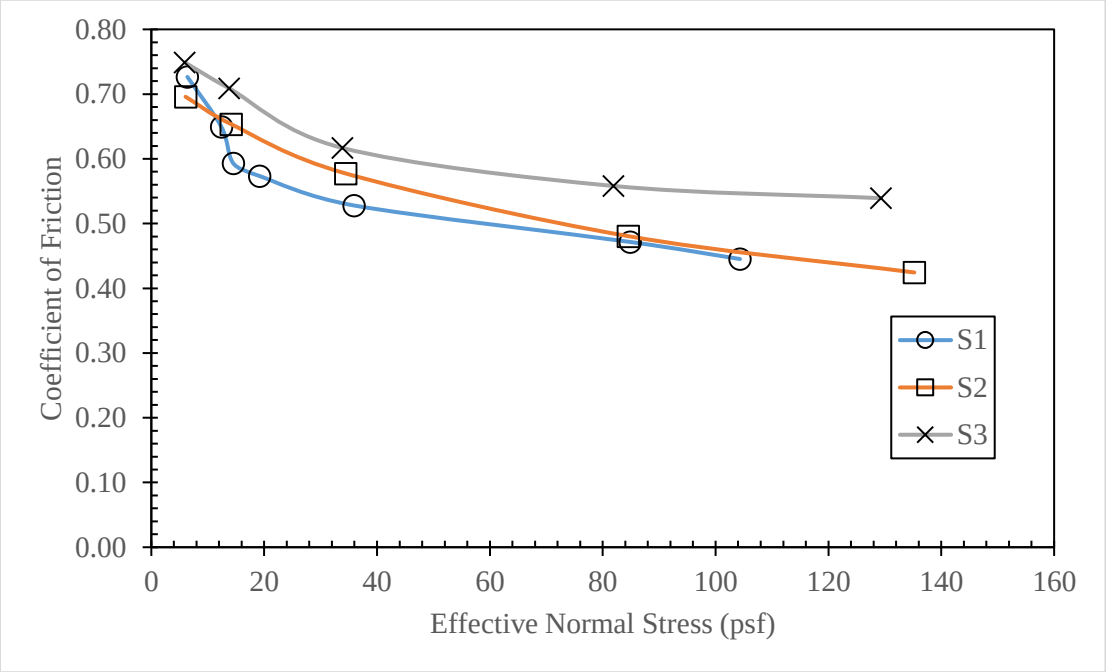

Figure 5.17 Coefficient of friction versus effective normal stress.

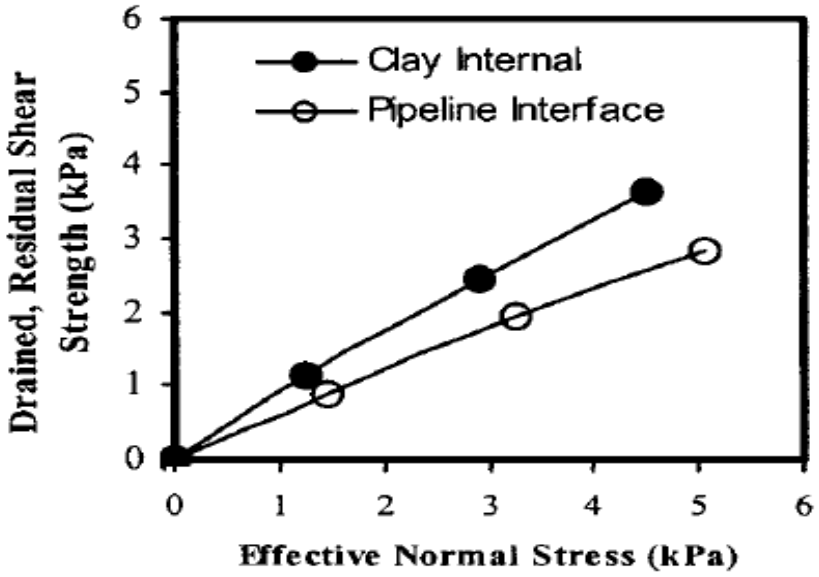

Figure 5.18 Variation of drained residual strength with effective normal stress (Najjar et al. 2007).

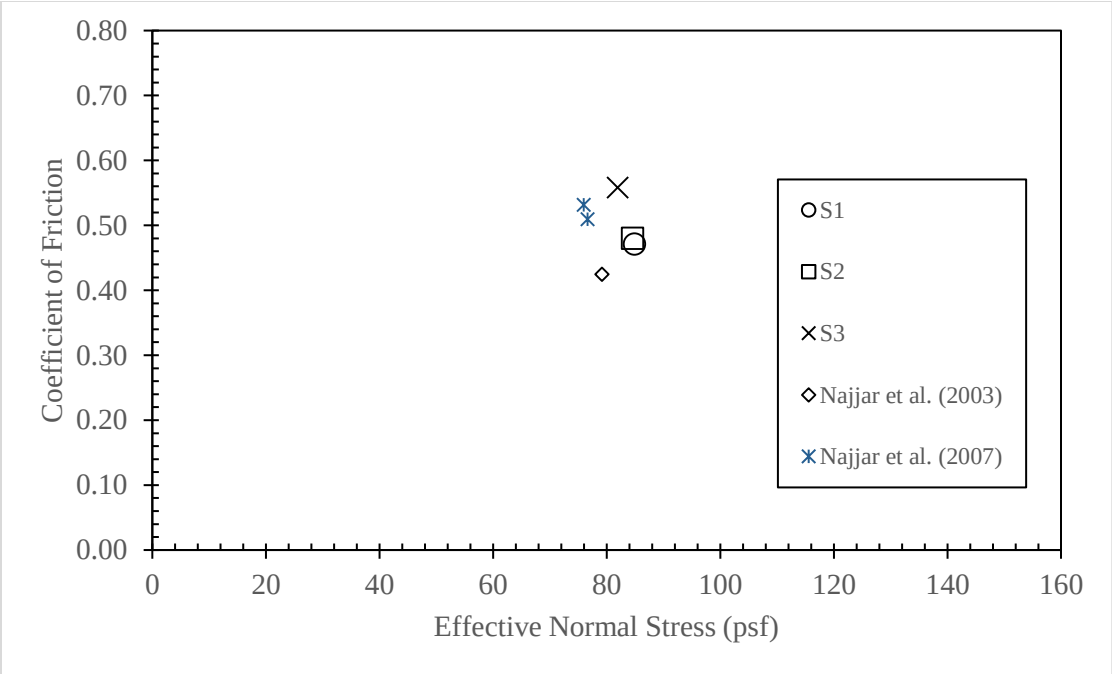

Figure 5.19 Comparison of coefficient of friction for similar soil and similar interface.

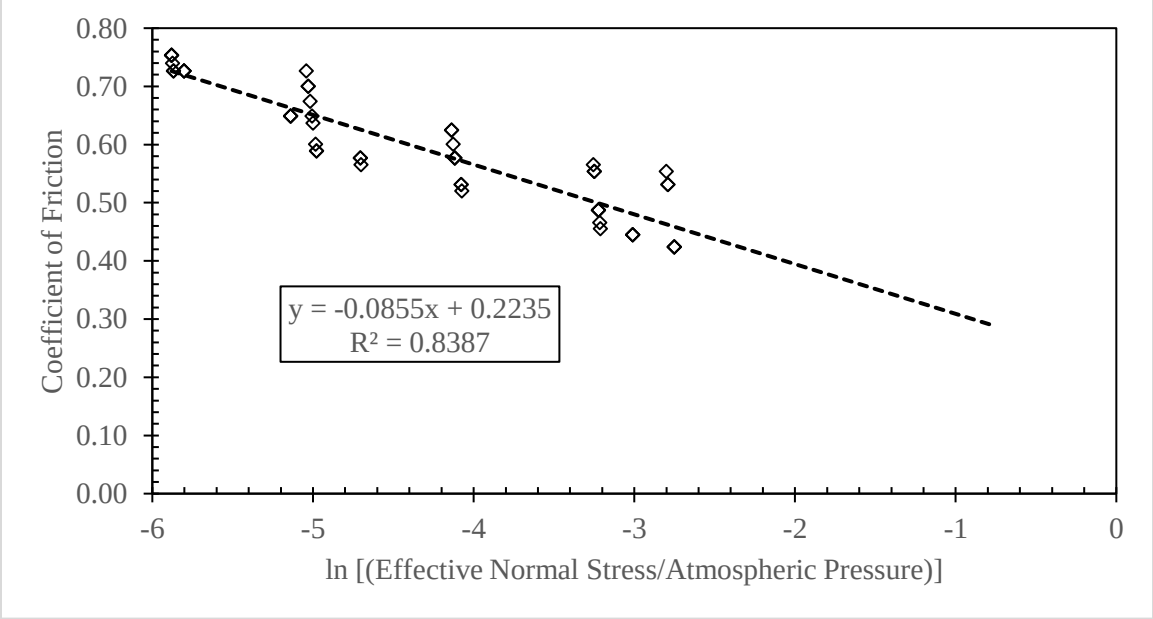

Figure 5.20 Coefficient of friction versus ln (effective normal stress/atmospheric pressure).

5.7 INFLUENCE OF COATING MANUFACTURER

Two additional tests were carried out using Interface 2, which is a smooth coating specified as the same material as the coating used in the previous tests but obtained from a different manufacturer. The results of these tests are shown in Table 5.6 along with tests results under similar conditions using Interface 1. The relative difference in the coefficient of friction can be up to approximately 18%, which indicates that coatings with same specifications, but from different manufacturers may present minor differences in performance and, depending on the case, this difference should be considered.

Table 5.6 Comparison of similar tests using Interface 1 and Interface 2

Interface	Soil Source	Effective Normal Stress on Horizontal Plane (psf)	Effective Normal Stress at Failure (psf)	Residual Shear Strength (psf)	Drained Residual Secant Friction Angle (deg)	Coefficient of Friction
1	S1	93.8	84.31	11.40	26.0	0.49
	S1	93.8	85.35	10.16	24.5	0.46
2	S1	93.8	86.97	8.24	22.0	0.40
	S1	93.8	86.97	8.24	22.0	0.40

5.8 CONCLUSIONS

A tilt table test method is described for measuring the drained residual strength of interfaces between flowlines and surrounding soils, in particular polypropylene interfaces and Gulf of Mexico clay. Based on results from 50 tests, the following conclusions can be drawn about the interface behavior:

1. The tilt-table results were found to be repeatable, generating similar results for tests performed under similar conditions.

2. The interface residual strength is mobilized at about 1 to 2 in (25 to 50mm) of shear displacement along the interface for 2-mm-thick specimens of normally consolidated clays, initially in remolded state, then consolidated and subjected to effective normal stresses less than 150psf (7.2kPa).

3. The Mohr-Coulomb failure envelope for the drained residual strength of the interface used in this study is non-linear for very low effective normal stresses and the curvature tends to be flatter as the stress increases.

4. The drained residual strength of the interface depends on the composition of the clay. Similar tests conducted using soils obtained from different locations yielded different results.

5. Results from creep tests indicate that the drained residual strength of interfaces obtained following the tilt-table procedures described in this study indeed corresponds to drained conditions. Additionally, there is no evidence of drained creep for time intervals less than 19 hours.

6. Results obtained from tests conducted with smooth coatings made of the same material and with similar specifications but obtained from different manufacturers differed up to about 18%. This may be due to possible discrepancies in the manufacturing process, causing the coating surfaces to be different not only in the microlevel, but also in the macrolevel.

7. An empirical correlation is proposed to estimate the drained residual strength of polypropylene interfaces when in contact with Gulf of Mexico clay. This correlation should not be used for design purposes, since the interface properties and the clay composition may vary significantly if compared to what was used in this study.

Chapter 6: Conclusions

Three different test methods are presented to characterize Gulf of Mexico clay at low effective normal stresses. T-bar tests were performed to measure the increase in the undrained shear strength of Gulf of Mexico clay for relatively short time intervals. Additionally, embedment tests were conducted using pipe sections with different lengths and the results were compared with the predicted values obtained using the methodology presented by Simpson et al. (2015) in the SAFEBUCK JIP and DNV-RPF110 merged guideline, which is the current standard of practice for predicting the initial penetration of subsea pipelines during the laying process. Moreover, a tilt-table method is described for measuring the drained residual strength of interfaces between flowlines and surrounding soils. A total of 50 tests were carried out using soil samples obtained from three different locations and a polypropylene coating, applying effective normal stresses ranging from approximately 7 psf (0.4 kPa) to 145 psf (7 kPa).

From the T-bar tests, the following conclusion can be drawn:

1. The results indicate that thixotropy of the clay has an impact on the undrained shear strength shortly after the clay is remolded. It is likely that a large portion of the increase in the undrained shear strength of the clay due to thixotropy occurs within 72 hours.
2. After approximately 72 hours, most of the tests indicate that sensitivity assumes a value of about 2. This value is within the range of values reported in the literature. Further studies need to be conducted in order to confirm if the undrained shear strength and the sensitivity still significantly increasing within 10 days after the clay has been mixed.
3. An empirical correlation between remolded undrained shear strength and water content is proposed. This relationship indicates that a decrease in about 20% in water content can cause an increase in $S_{u,r}$ of approximately 300%.

4. The sensitivity does not seem to vary with depth shortly after the clay has been remolded. However, for sensitivity values greater than 1.5, it seems to slightly decrease as depth increases.

From the embedment test, the following conclusions can be drawn:

5. The method outlined in Simpson et al. (2015) for estimating initial embedment performed well for the 3-ft long pipe and provides a good starting point for predicting the embedment of larger pipes where the pipe unit weight can be controlled.

6. The initial embedment can be treated as a bearing capacity failure of the supporting soil and the method presented by Simpson et al. (2015) only provides an estimate of the initial vertical displacement. This estimation does not account for settlement of the clay due consolidation following the laying process. Thus, the settlement following installation must be considered when estimating the final settlement of the pipe.

7. A theoretical consolidation curve (c_v = 0.009 ft^2/day) with final settlement 10% greater than the measured settlement agrees well with measured settlement curves, indicating that a significant part of the consolidation seems to occur a few weeks after the pipe is laid on the soil bed. This value of c_v is consistent with values reported in the literature for Gulf of Mexico clay at shallow depths.

8. The coefficient of compression is estimated based on the initial penetration and the settlement curves. The values range from 0.71 to 1.26, with an average value of 0.78. This wide range may be due to the assumptions used to estimate C_c and the uncertainties associated with hand-placing the pipe on the soil surface.

From the tilt-table tests, the following conclusions can be drawn:

9. The tilt-table method is of potential use for measuring the drained residual strength at low effective normal stresses for interfaces between soils and flowlines. The results were found to be repeatable.

10. The interface residual strength is mobilized at about 1 to 2 in (25 to 50mm) of shear displacement along the interface for 0.08 in-thick (2 mm) specimens of normally consolidated clays, initially in remolded state, subjected to effective normal stresses less than 150 psf (7.2 kPa).

11. The Mohr-Coulomb failure envelope for the drained residual strength of the interface used in this study is non-linear for very low effective normal stresses and the curvature becomes flatter as the stress increases.

12. The drained residual strength of the interface depends on the composition of the clay.

13. Results from creep tests indicate that the drained residual strength of interfaces obtained following the tilt-table procedures described in this study indeed corresponds to drained conditions. No evidence of drained creep was observed within a time interval of 19 hours.

14. Similar coatings obtained from different manufacturers may present minor differences in performance under same stress conditions.

15. An empirical correlation is proposed to estimate the drained residual interface strength between Gulf of Mexico clay and polypropylene coatings.

Appendices

APPENDIX A - T-BAR CURVES (S_U VERSUS DEPTH) FOR GROUPS A, B AND C

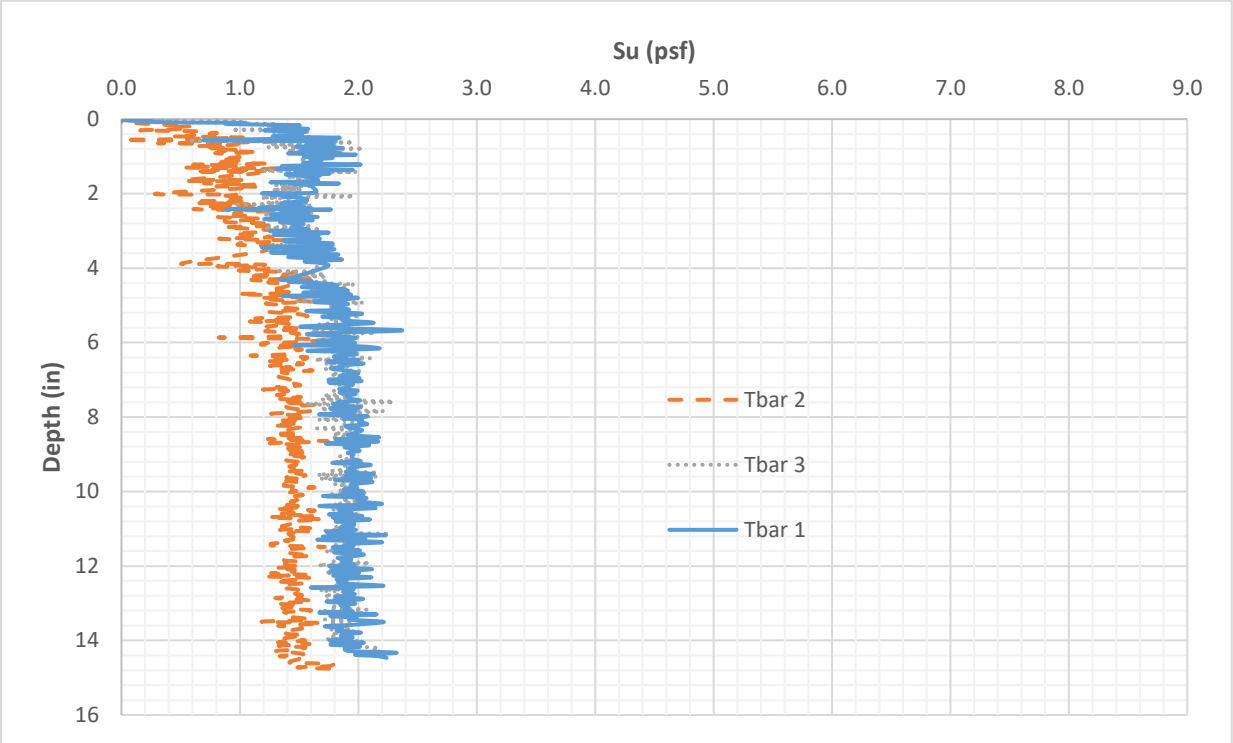

Figure A.1 Test 1A

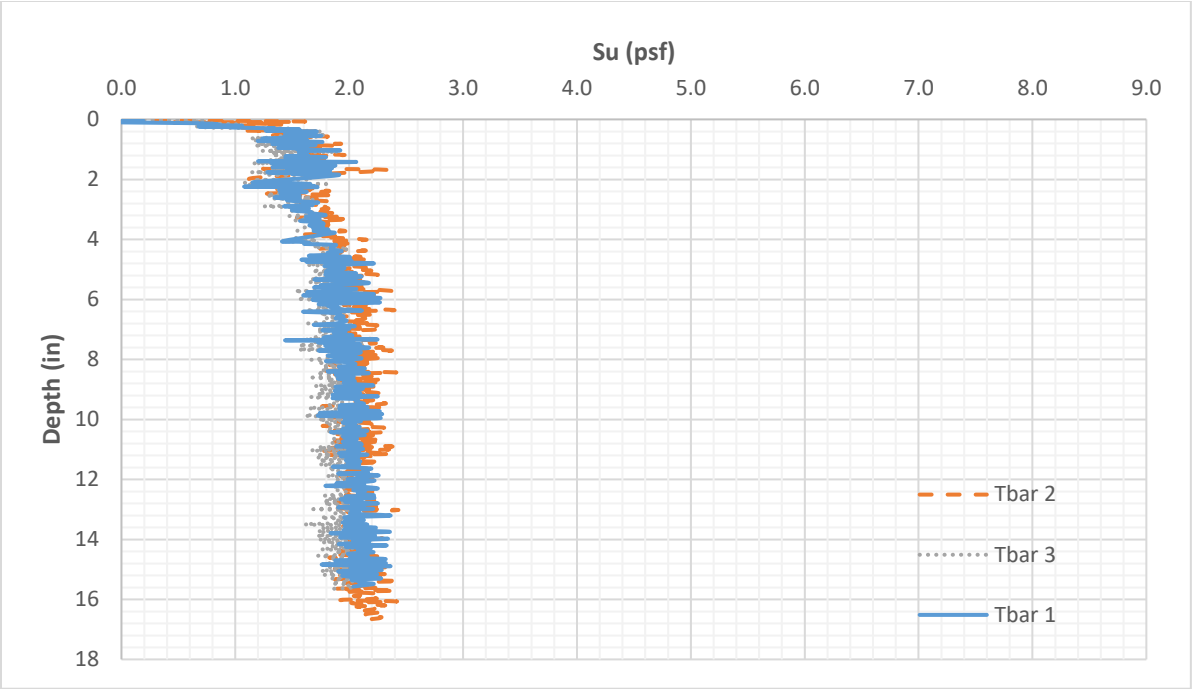

Figure A.2 Test 2A

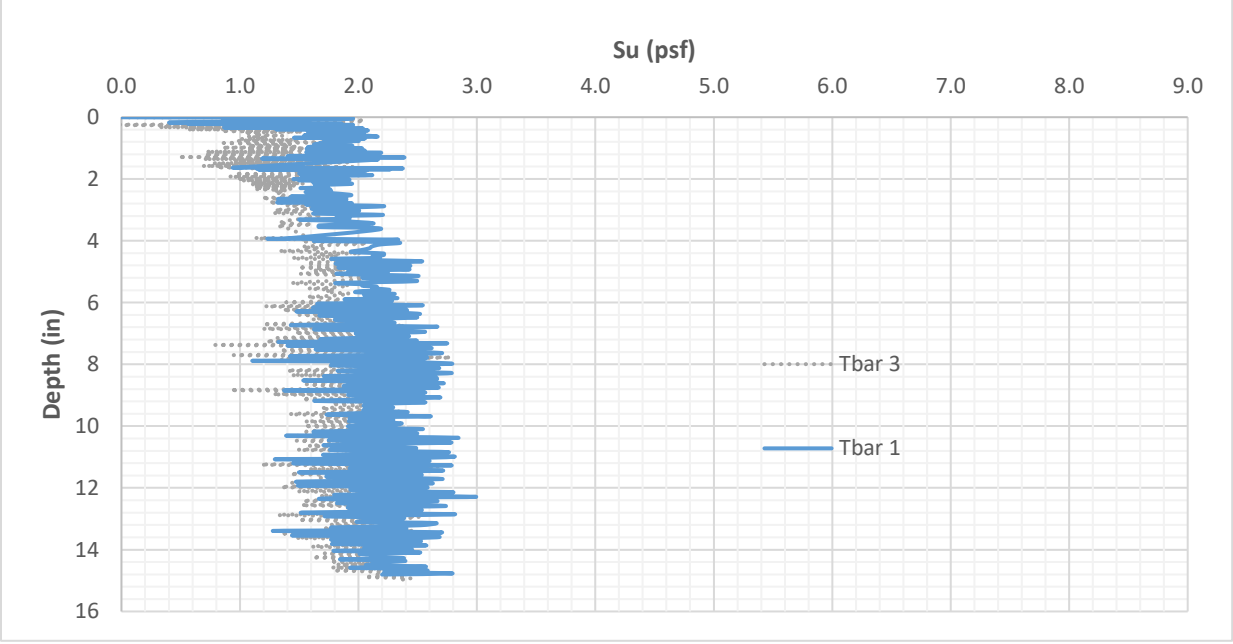

Figure A.3 Tests 3A

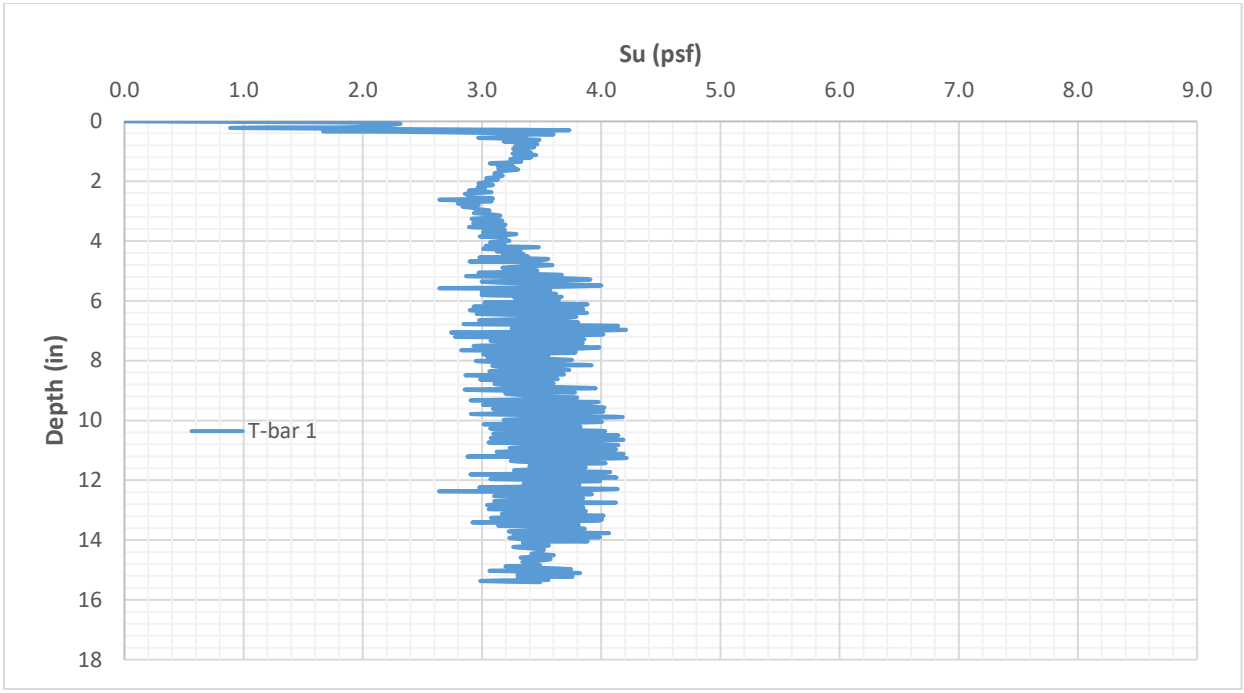

Figure A.4 Test 4A

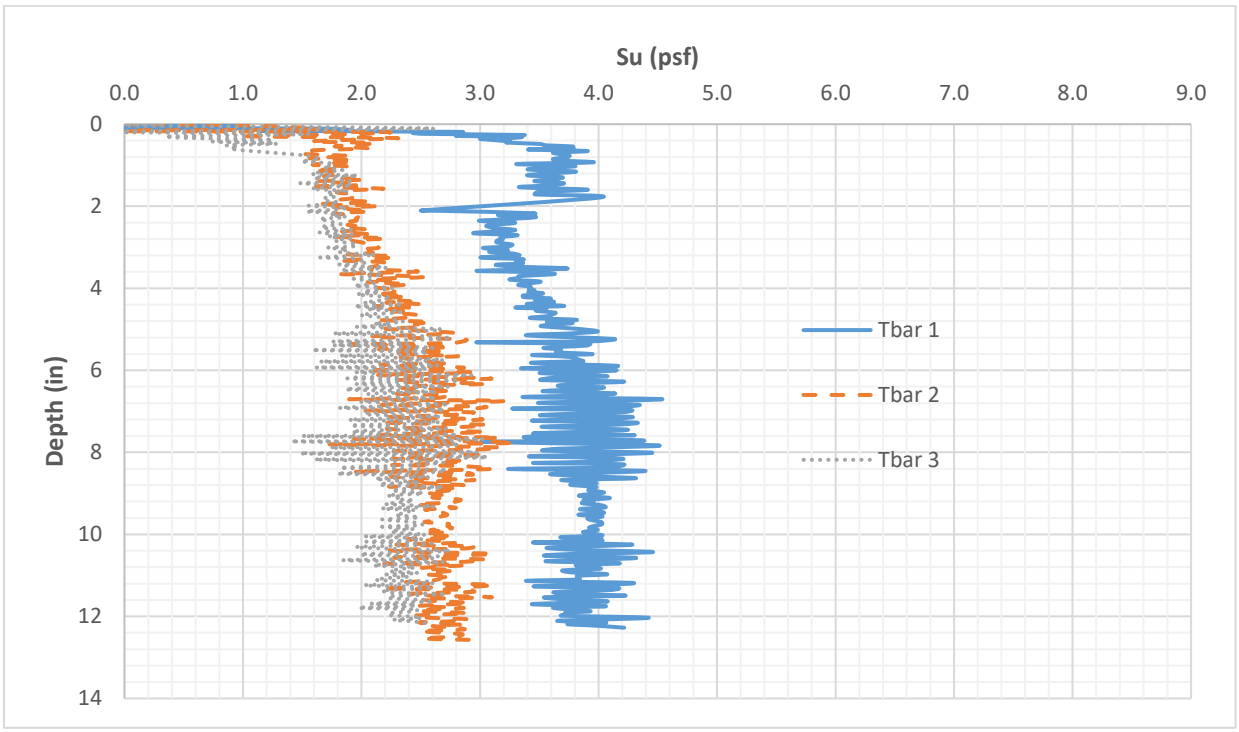

Figure A.5 Test 5A

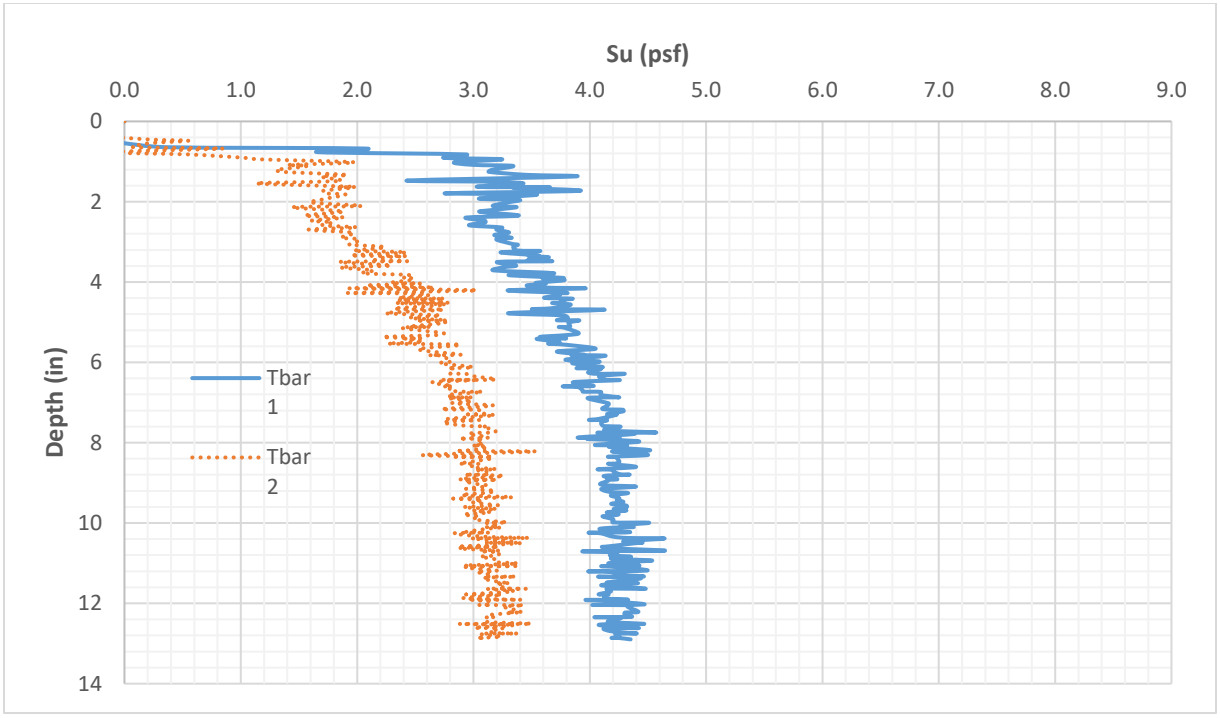

Figure A.6 Test 6A

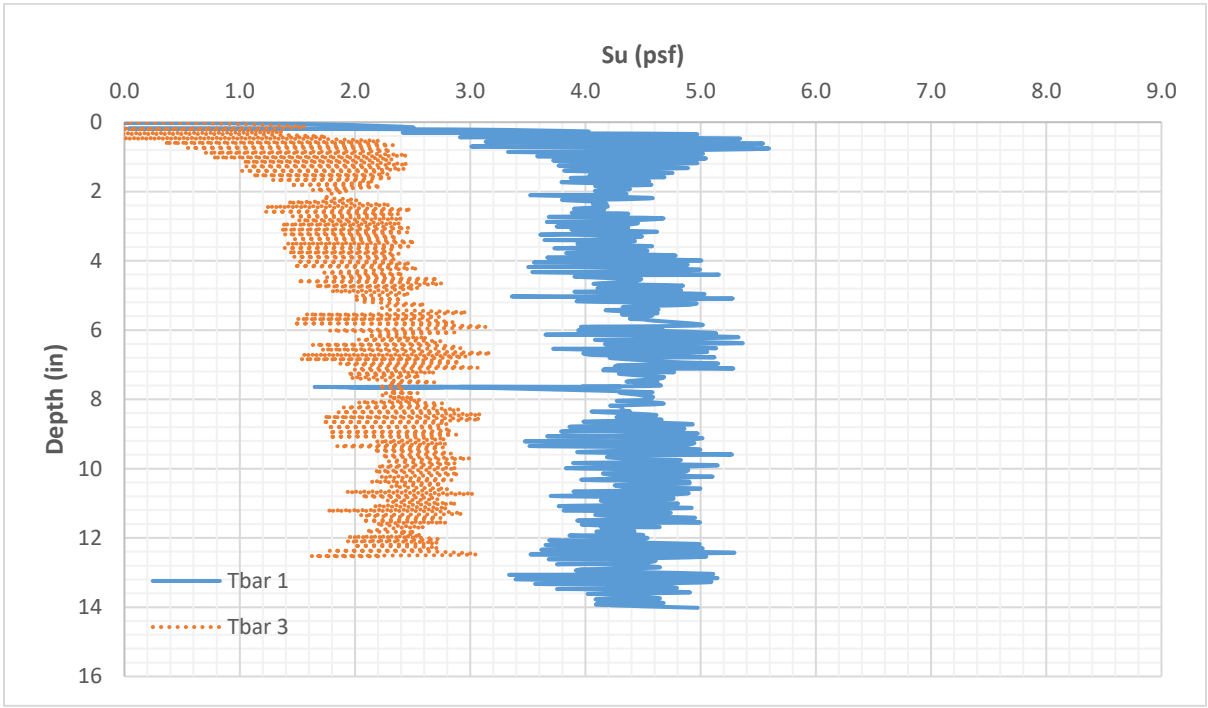

Figure A.7 Test 7A

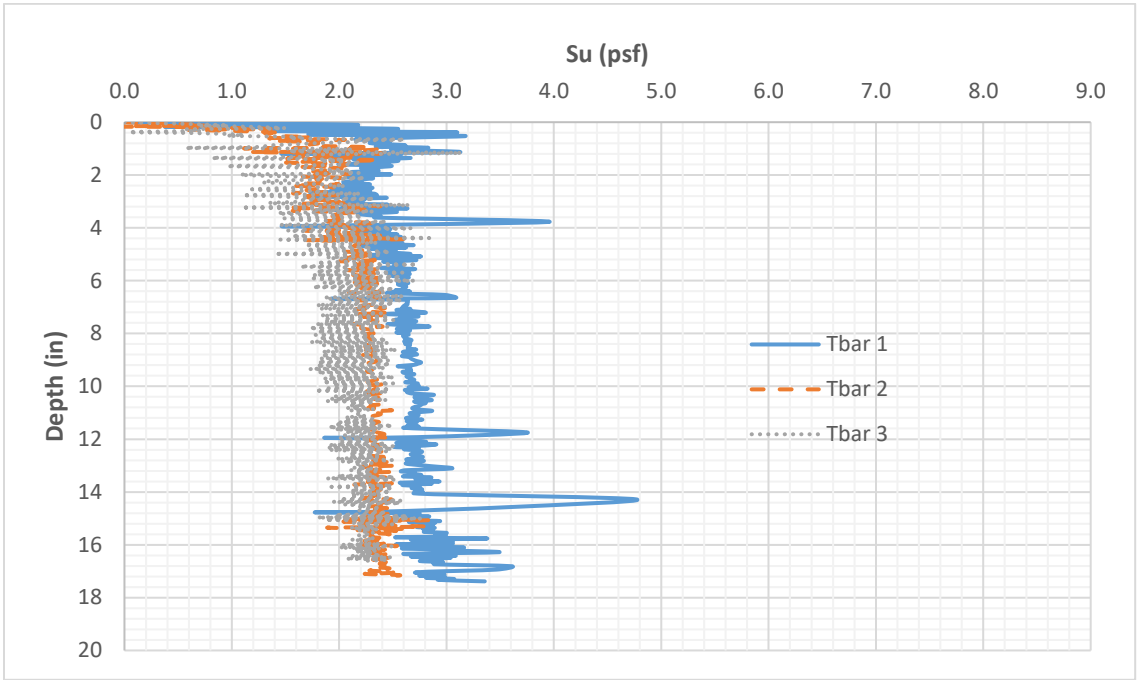

Figure A.8 Test 1B

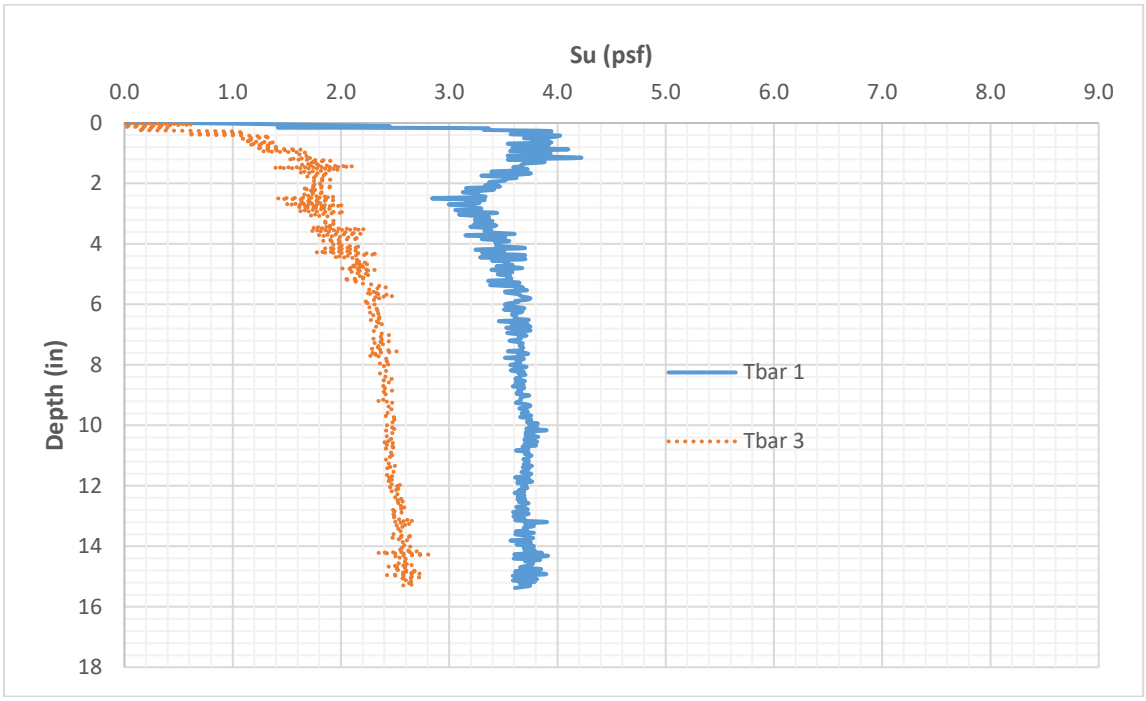

Figure A.9 Test 2B

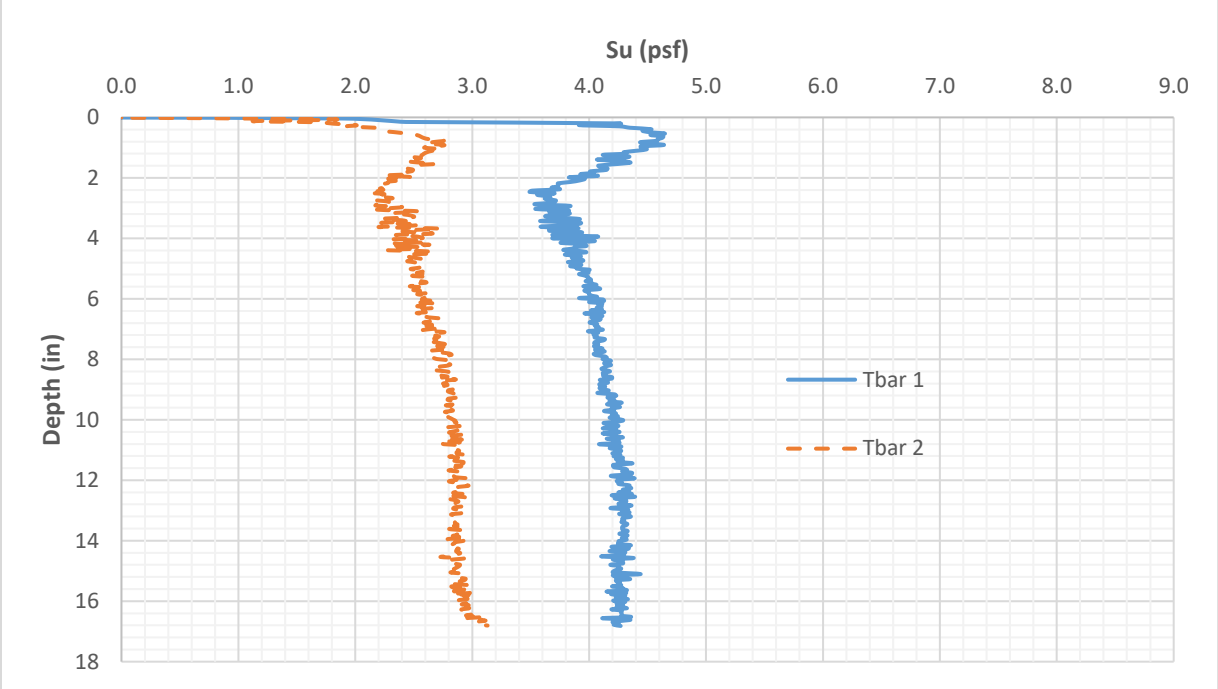

Figure A.10 Test 3B

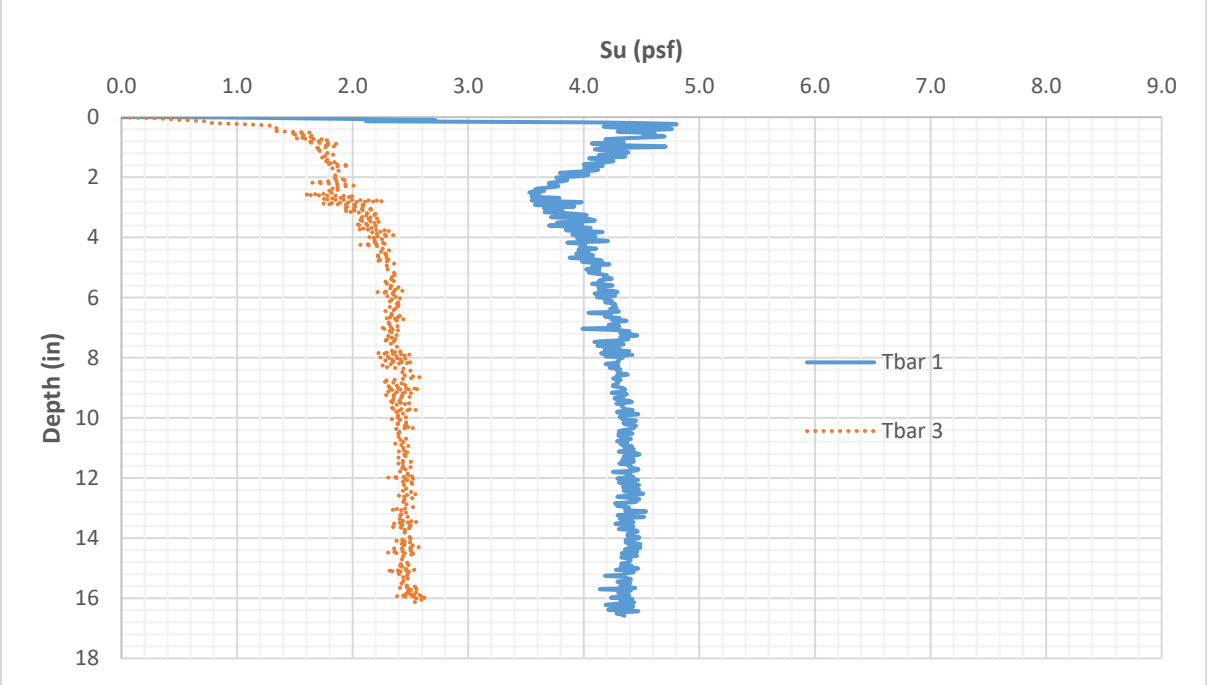

Figure A.11 Test 4B

APPENDIX B – TILT-TABLE TESTS

Table B. 1 Detailed Test Program.

Test Number	Soil Source	Effective Normal Stress on Horizontal Plane (psf)	Effective Normal Stress on Horizontal Plane (kPa)	Initial Water Content (%)	Final Water Content (%)
1	S1	7.9	0.4	172	122
2	S1	7.9	0.4	165	125
3	S1	7.9	0.4	163	122
4	S1	14.8	0.7	169	#N/A
5	S1	14.8	0.7	174	#N/A
6	S1	14.8	0.7	166	#N/A
7	S1	16.9	0.8	158	111
8	S1	16.9	0.8	154	113
9	S1	16.9	0.8	152	110
10	S1	22.1	1.1	153	#N/A
11	S1	22.1	1.1	157	#N/A
12	S1	22.1	1.1	151	#N/A
13	S1	40.6	1.9	154	94
14	S1	40.6	1.9	148	102
15	S1	40.6	1.9	149	97
16	S1	93.8	4.5	138	84
17	S1	93.8	4.5	136	84
18	S1	114.2	5.5	145	77
19	S1	114.2	5.5	#N/A	79
20	S1	114.2	5.5	142	#N/A
21	S2	7.4	0.4	221	153
22	S2	7.4	0.4	205	151
23	S2	7.4	0.4	207	152
24	S2	16.9	0.8	217	139
25	S2	16.9	0.8	212	141
26	S2	16.9	0.8	218	138
27	S2	39.8	1.9	188	117
28	S2	39.8	1.9	186	127
29	S2	39.8	1.9	206	121
30	S2	93.8	4.5	201	104
31	S2	93.8	4.5	205	103
32	S2	93.8	4.5	163	109
33	S2	146.9	7.1	207	95
34	S2	146.9	7.1	201	97
35	S2	146.9	7.1	204	95
36	S3	7.4	0.4	289	173
37	S3	7.4	0.4	160	171
38	S3	7.4	0.4	165	175
39	S3	16.9	0.8	225	155
40	S3	16.9	0.8	232	158
41	S3	16.9	0.8	234	151
42	S3	39.8	1.9	#N/A	#N/A
43	S3	39.8	1.9	#N/A	#N/A
44	S3	39.8	1.9	#N/A	#N/A
45	S3	93.8	4.5	228	136
46	S3	93.8	4.5	#N/A	#N/A
47	S3	93.8	4.5	271	132
48	S3	146.9	7.1	205	119
49	S3	146.9	7.1	208	#N/A
50	S3	146.9	7.1	201	116.4

Table B. 2 Detailed Test Results.

Test Number	Soil Source	Effective Normal Stress on Horizontal Plane (psf)	Drained Residual Secant Friction Angle (deg)	Coefficient of Friction	Effective Normal Stress at Failure (psf)	Residual Shear Strength (psf)	σ'/Pa	ln(σ')
1	S1	7.9	36.0	0.73	6.4	4.6	0.003	-5.80
2	S1	7.9	36.0	0.73	6.4	4.6	0.003	-5.80
3	S1	7.9	36.0	0.73	6.4	4.6	0.003	-5.80
4	S1	14.8	33.0	0.65	12.4	8.1	0.006	-5.14
5	S1	14.8	33.0	0.65	12.4	8.1	0.006	-5.14
6	S1	14.8	33.0	0.65	12.4	8.1	0.006	-5.14
7	S1	16.9	31.0	0.60	14.5	8.7	0.007	-4.98
8	S1	16.9	30.5	0.59	14.6	8.6	0.007	-4.98
9	S1	16.9	30.5	0.59	14.6	8.6	0.007	-4.98
10	S1	22.1	30.0	0.58	19.1	11.1	0.009	-4.71
11	S1	22.1	29.5	0.57	19.2	10.9	0.009	-4.70
12	S1	22.1	30.0	0.58	19.1	11.1	0.009	-4.71
13	S1	40.6	28.0	0.53	35.8	19.1	0.017	-4.08
14	S1	40.6	28.0	0.53	35.8	19.1	0.017	-4.08
15	S1	40.6	27.5	0.52	36.0	18.7	0.017	-4.07
16	S1	93.8	24.5	0.46	85.4	38.9	0.040	-3.21
17	S1	93.8	26.0	0.49	84.3	41.1	0.040	-3.22
18	S1	114.2	24.0	0.45	104.3	46.4	0.049	-3.01
19	S1	114.2	24.0	0.45	104.3	46.4	0.049	-3.01
20	S1	114.2	24.0	0.45	104.3	46.4	0.049	-3.01
21	S2	7.4	37.0	0.75	5.9	4.5	0.003	-5.88
22	S2	7.4	36.0	0.73	6.0	4.3	0.003	-5.87
23	S2	7.4	36.0	0.73	6.0	4.3	0.003	-5.87
24	S2	16.9	32.5	0.64	14.3	9.1	0.007	-5.00
25	S2	16.9	33.0	0.65	14.2	9.2	0.007	-5.01
26	S2	16.9	34.0	0.67	14.0	9.5	0.007	-5.02
27	S2	39.8	30.0	0.58	34.5	19.9	0.016	-4.12
28	S2	39.8	30.0	0.58	34.5	19.9	0.016	-4.12
29	S2	39.8	30.0	0.58	34.5	19.9	0.016	-4.12
30	S2	93.8	26.0	0.49	84.3	41.1	0.040	-3.22
31	S2	93.8	25.0	0.47	85.0	39.6	0.040	-3.21
32	S2	93.8	26.0	0.49	84.3	41.1	0.040	-3.22
33	S2	146.9	23.0	0.42	135.2	57.4	0.064	-2.75
34	S2	146.9	23.0	0.42	135.2	57.4	0.064	-2.75
35	S2	146.9	23.0	0.42	135.2	57.4	0.064	-2.75
36	S3	7.4	37.0	0.75	5.9	4.5	0.003	-5.88
37	S3	7.4	36.5	0.74	5.9	4.4	0.003	-5.87
38	S3	7.4	37.0	0.75	5.9	4.5	0.003	-5.88
39	S3	16.9	36.0	0.73	13.7	9.9	0.006	-5.04
40	S3	16.9	35.0	0.70	13.8	9.7	0.007	-5.03
41	S3	16.9	35.0	0.70	13.8	9.7	0.007	-5.03
42	S3	39.8	31.00	0.60	34.1	20.5	0.016	-4.13
43	S3	39.8	32.00	0.62	33.8	21.1	0.016	-4.14
44	S3	39.8	32.00	0.62	33.8	21.1	0.016	-4.14
45	S3	93.8	29.0	0.55	82.0	45.5	0.039	-3.25
46	S3	93.8	29.0	0.55	82.0	45.5	0.039	-3.25
47	S3	93.8	29.5	0.57	81.6	46.2	0.039	-3.26
48	S3	146.9	28.0	0.53	129.7	69.0	0.061	-2.79
49	S3	146.9	29.0	0.55	128.5	71.2	0.061	-2.80
50	S3	146.9	28.0	0.53	129.7	69.0	0.061	-2.79

References

1. Aubeny, C.P., Shi, H. & Murff. J.D. (2005). 'Collapse loads for a cylinder embedded in trench in cohesive soil'. *Int. J. of Geomechanics*, ASCE, 5(4), 320-325.

2. Bae, S. (2009). "Drained residual shear and interface strength of soils at low effective normal stress". *Master Thesis*, The University of Texas at Austin.

3. Byrne, R. J., Kendall, J., and Brown, S. _1992_. "Cause and mechanism of failure, Kettleman Hills Landfill B-19, Phase IA." *Proc., Stability and Performance of Slopes and Embankments-II*, ASCE, New York, 1188–1215.

4. Chandler, R. J., and Hardie, T. N. (1989). "Thin-sample technique of residual strength measurement." *Geotechnique*, 39_3_, 527–531.

5. FUGRO (2005). "*Geotechnical investigation, Chevron Gulf of Mexico gas hydrates Jip, Blocks 13 and 14, Atwater valley area, block 151, Keathley canyon area, Gulf of Mexico: Results of core sample analysis, standard and advanced laboratory testing*". Report No. 0201-5081, CHEVRON TEXACO ENERGY TECHNOLOGY COMPANY, Houston, Texas.

6. Chung, S.F. and Randolph, M.F. (2004) 'Penetration resistance in soft clay for different shaped penetrometers'. *Proc. Int. Conf. Site Characterisation*, Porto, Portugal, 1: 671-678.

7. Dejong, J., Yafrate, N., DeGroot, D., Low, H. E. & Randolph, M. F. (2010). Recommended practice for full-flow penetrometer testing and analysis. *Geotech. Testing J. ASTM* **33**, No. 2, paper ID GTJ102468.

8. Fang, Y. S., Chen, T. J., Holtz, R. D., and Lee, W. F. _2004_. “Reduction of boundary friction in model tests.” *Geotech. Test. J.*, 27_1_, 1–10.

9. Finnie, I. M. S., Randolph, M. F., “Punch-Though and liquefaction induced failure on shallow foundations on calcareous sediments”, In: *Proceeding International Conference on Behaviour of Off-Shore Structures – BOSS ’94*, Boston, v. 1, pp. 217-230, 1994.

10. Fox, P. J., and Stark, T. D. _2004_. “State-of-the-art report: GCL shear strength and its measurement.” *Geosynthet. Int.*, 11_3_, 141–175.

11. Francisca, F., C. Ruppel., T.-T. Yun., Santamarina, J. C. (2005). Geophysical and geotechnical properties of near-seafloor sediments in the northern Gulf of Mexico gas hydrate province”. *Earth and Planetary Science Letters*, Vol. 237, 924-939.

12. Gerkus, H., (2016). “Model experiments to measure yield thresholds and trajectories for plate anchors and develop a new anchor concept”. *PhD Dissertation*, The University of Texas at Austin.

13. Gibson, R. E., and Henkel, D. J. _1954_. “Influence of duration of tests at constant rate of strain on measured drained strength.” *Geotechnique*, 4_1_, 6–15.

14. Gilbert, R. B., and Byrne, R. J. _1996_. “Strain-softening behavior of waste containment system interfaces.” *Geosynthetics. Int.*, 3(2), 2–23.

15. Gilbert, R. B., Wright, S. G., Shields, K. M., and Obermeyer, J. E. _2004_. “Lower-bound shear strength for geosynthetic clay liners in base liners.” *Geosynthetics. Int.*, 11(3), 200–211.

16. Gilbert, R. B., Aubeny, C. P., Chen, C.-H., McCarthy, K. B., & Vilkki, J. (2012). Experimental and Analytical Modeling for Drag Anchors. Final Report Prepared for ABS Consulting, Project No. ABSC/1514096/DM-06 Offshore Technology Research Center Project 32558-B2930.

17. House, A. R., Oliveira, J. R. M. S., Randolph, M. F., (2001). 'Evaluating the Coefficient of Consolidation Using Penetration Tests', *The International Journal of Physical Modelling in Geotechnics,* v. 1, n. 3, 17-26.

18. Huang, Y. (2015). "Designing a laboratory model test program for developing a new offshore anchor". *Master Thesis*. The University of Texas at Austin.

19. Jeanjean, P. Andersen, K. H., & Kalsnes, B. (1998). "Soil parameters for design of suction caissons for Gulf of Mexico deepwater clays". *Offshore Technology Conference*. Doi: 10.4043/8830-MS.

20. Krost, K., Gourvenec, S., and White, D. (2010). 'Consolidation around partially embedded submarine pipelines'. *Geotechnique,* DOI: 10.1680/geot.8.T.015.

21. Lai, Y. (2017). "Laboratory model tests on drag and dynamically embedded plate anchors in layered clay profiles". *PhD Dissertation*, The University of Texas at Austin.

22. Lee, C. H. (2008). "Constructing test beds of clay with a specified profile of undrained shear strength versus depth". *Master Thesis,* The University of Texas at Austin,.

23. Lehane, B. M., and Jardine, R. J. _1992_. "Residual strength characteristics of Bothkennar clay." Geotechnique, 42(2), 363–367.

24. Lemos, L. J. L., and Vaughan, P. R. (2000). "Clay-interface shear resistance." *Geotechnique*, 50(1), 55–64.

25. Liu, C. N., Gilbert, R. B., Thiel, R. S., and Wright, S. G. (1997). "What is an appropriate factor of safety for landfill cover slopes?" *Proc., Geosynthetics '97*, IFAI, Roseville, Minn., 481–496.

26. Low, H.E., Lunne, T., Andersen, K.H., Sjursen, M.A., Li, X. and Randolph, M.F. (2010) 'Estimation of intact and remoulded undrained shear strength from penetration tests in soft clays'. *Geotechnique*, 10(11): 843-859.

27. Madhuri, M., Biscontin, G. (2014). "Geotechnical characterization of Gulf of Mexico clay". ASME. International Conference on Offshore Mechanics and Artic Engineering, Volume 3: *Offshore Geotechnics* ():V003T10A019. Doi:10. 1115/OMAE2014-24183.

28. McCarron, William & Been, Ken & Clukey, Edward & Doyle, Earl & Gilbert, Robert & Kasch, Vernon & Murff, James & Palmer, Andrew & Randolph, Mark & Rivette, Jill & Young, Alan. (2011). *Deepwater Foundations and Pipeline Geomechanics*.

29. Merril, K.S., and O'Brien, A. J., 1997, 'Strength and conformance testing of a GCL in a solid waste landfill lining system'. *Testing and Acceptance Criteria for Geosynthetic Clay Liners, ASTM STP 1308*, L. W. Weill, Ed., 71-88.

30. Najjar, S. S., Gilbert, R. B., Liedtke, E. A., and McCarron, B. _2003_. "Tilt table test for interface shear resistance between flowlines and soils." *Proc., Int. Conf. on Offshore Mechanics and Arctic, Engineering—OMAE, Vol. 3*, ASME, Cacun, Mex., 859–866.

31. Najjar, S. S., R. B. Gilbert, E. Liedtke, B. McCarron, A. G. Young. (2007). "Residual shear strength for interfaces between pipelines and clays at low effective normal stresses". *Journal of Geotechnical and Geoenvironmental Engineering* 133(6): 695-706.

32. Norena, PC. T., (2015). “Soil-pipe cyclic interaction in soft clay: physical modeling in centrifuge”. *PhD dissertation*, Federal University of Rio de Janeiro.

33. NORSOK (2004). NORSOK *standard: Marine soil investigations,* G-001, Rev. 2. Lysaker: Standards Norway.

34. Pederson, R. C., Olson, R. E., and Rauch, A. F. _2003_. “Shear and interface strength of clay at very low effective stress.” *Geotech. Test. J.,* 26(1), 71–78.

35. Randolph, M. F. (2004). Characterisation of soft sediments for offshore applications, *Keynote Lecture. Proc. 2nd Int. Conf. Site Characterisation,* Porto 1, 209–231.

36. Randolph, M. F., Hope, S., (2004) ‘Effect of cone velocity on cone resistance and excess pore pressures’. In: *Proceedings of the International Symposium on Engineering Practice and Performance of Soft Deposits*, Yodogawa Kogisha, Osaka, Japan, 147-152.

37. Randolph, M. F., White, D. J., (2008) ‘Pipeline embedment in deep water: processes and quantitative assessment’. *Proc. Annu. Offshore Technology Conference*, Houston, Texas, Paper OTC19128, 2-16.

38. Randolph, M.F., Guadin, C., Gourvenec, S.M., White, N.B., Cassady, M.J. (2011) ‘Recent advances in offshore geotechnics for deep water oi and gas developments’. *Ocean Engineering* 38(11) 818-834.

39. Randolph, M.F., & Gourvenec, S.M, (2011), “Offshore geotechnical engineering”, Spon press, first published in 2011. ISBN 978-0-415-47744-4.

40. Richardson, G. E., Nixon, L. D., Kazanis, E. G., Montgomery, T. M., & Gravois, M. P. (2008). Deepwater Gulf of Mexico 2008: America's Offshore Energy Future. *Vols.*

2008-013. New Orleans, LA: U.S. Department of the Interior, Minerals Management Service, Gulf of Mexico OCS Region.

41. Simpson, N., Guinard, M., Cosham, A., Røneid, S., and Bergseng K. (2015). Merger of SAFEBUCK and DNV-RP-F110.

42. Stark, T. D., and Poeppel, A. R. _1994_. "Landfill liner interface strengths from torsional-ring-shear tests." J. Geotech. Engrg., 120(3), 597–615.

43. Stewart, D.P., and Randolph, M.F. 1991. A new site investigation tool for the centrifuge. In Proceedings of the International Conference on Centrifuge Modelling, Centrifuge '91, Boulder, Colo., 13–14 June 1991. Balkema, Rotterdam, the Netherlands. pp. 531–538.

44. Stewart, D.P. & Randolph, M.F. (1994). T-bar penetration testing in soft clay. *J. Geotechnical Eng., ASCE,* 120(12):2230-2235.

45. Taukoor, V. and Rutherford, C.J. (2016). "Displacement rate effects during T-bar cycling in remoulded Gulf of Mexico clay". *Geotechnique*, Vol. 67(6), 553-557. DOI: 10.1680/jgeot.16.P.078.

46. Taukoor, V. and Rutherford, C.J., & Olson, S. M. (2018). "Post-cyclic behavior of a Gulf of Mexico clay". *Geotechnical Earthquake Engineering and Soil Dynamics Conference, 345-356.* https://doi.org/10.1061/9780784481486.036.

47. Taukoor, V. and Rutherford, C.J., & Olson, S. M. (2019). "Cyclic behavior of a reconstituted Gulf of Mexico clay". *Geo-Congress: Earthquake Engineering and Soil Dynamics*, 313-321. https://doi.org/10.1061/9780784482100.032

48. Tika-Vassilikos, T. (1991). “The clay-on-steel ring shear tests and their implications for displacement piles.” *Geotech. Test. J.*, 14(4), 457– 463.

49. Tsubakihara, Y., and Kishida, H. (1993a). “Frictional behavior between normally consolidated clay and steel by two direct shear type apparatuses.” *Soils Found.*, 33(2), 1–13.

50. Tsubakihara, Y., Kishida, H., and Nishiyama, T. (1993b). “Friction between cohesive soil and steel.” *Soils Found.*, 33(2), 145–156.

51. Westgate, Z., White, D.K. and Randolph, M.F. (2009) ‘Video observations of dynamic embedment during pipelaying on soft clay’. *Proc. Int. Conf. Offshore Mech. Artic. Eng.* (*OMAE*), Honolulu, Hawaii, Paper OMAE2009-79814.

52. White, D.J. and Randolph, M.F. (2007) ‘Seabed characterisation and models for pipeline-soil interaction’. *Int. J. Offshore Polar Eng.*, 17(3): 193-204.

53. White, D.J., Gaudin, C., Boylan, N., and Zhou, H. (2010) ‘Interpretation of T-bar penetrometer tests at shallow embedment and in very soft soils’. *Can Geotech. J.*, 47(2): 218-229.

54. Yafrate, N. J., Dejong, J. T., Degroot, D. J., Randolph, M. F., “Evaluation of Remolded Shear strength and Sensitivity of Soft Clay using Full-Flow Penetrometers”, **Journal of Geotechnical and Geoenvironmental Engineering**, pp. 1179 – 1189, 2009.

55. Zhou, H. and Randolph, M.F. (2009) “Resistance of full-flow penetrometers in rate-dependent and strain-softening clay’. *Geotechnique*, 59(2): 79-86.